EUROPEAN ORGANIZATION FOR PARTICLE PHYSICS

VELO Telescope Resolution and Efficiency Measurements

Paolo Bartalini[1], Jan Buytaert[2], Matthew Charles[3], Paula Collins[2], Hans Dijkstra[2], Olivier Dormond[1], Markus Elsing[2], Massimiliano Ferro-Luzzi[2], Frank Fiedler[2], Raymond Frei[1], Guido Gagliardi[1], Paweł Jałocha[4], Tjeerd Ketel[5], Patrick Koppenburg[1], Jim Libby[2], Chris Parkes[6], Ulrich Parzefall[6], Thomas Ruf[2], David Steele[1], Malica Tareb[1], Frederic Teubert[2], Mariusz Witek[4], and Victoria Wright[6]

[1] Insitut de Physique des Hautes Energies, Université de Lausanne, Bâtiment des Sciences Physiques, Dorigny, CH-1015 Lausanne
[2] European Laboratory for Particle Physics (CERN), Route de Meyrin 385, CH-1211 Genève
[3] Nuclear Physics Laboratory, University of Oxford, 1, Keble Road, Oxford OX1 3NP, GB
[4] Department of High Energy Physics, H. Niewodniczański Institute of Nuclear Physics, ulica Radzikowskiego 152, PL-31 342 Kraków
[5] Vrije Universiteit (VU), De Boelelaan 1079, NL-1007 MC Amsterdam
[6] University of Liverpool, Chadwick Building, Peach Street, Liverpool L69 7ZF, GB

Abstract

The 1998 prototypes for the LHCb Vertex Locator were characterised in a beam test. The efficiency of the detectors was studied as a function of bias voltage. For two different strip pitches, the resolution was determined as a function of the incident angle of the particles, with the following best resolutions:

strip pitch:	incident angle:	resolution:
$40\,\mu$m	$80 - 120$ mrad	$3.6 - 3.9\,\mu$m
$60\,\mu$m	≥ 200 mrad	$4.0 - 4.6\,\mu$m

The charge sharing fraction between adjacent strips was measured to be 5.3% for $40\,\mu$m pitch and 4.7% for $60\,\mu$m pitch, respectively. The results were compared with the LHCb simulation package SICb, and were used to test an improved simulation which is planned to replace the current LHCb Monte Carlo model.

1   Introduction

The 1998 prototype detectors for the LHCb Vertex Locator (VELO) are 300μm thick 72^0 wedge Hamamatsu n-on-n silicon detectors. In this study they are characterised in terms of their resolution and efficiency performance. Both of these parameters are essential for the future operation of the VELO testbeam, where these Hamamatsu detectors will be installed in a telescope setup for the investigation of new VELO prototypes. The knowledge of the resolution as a function of the angle of the tracks will be important both for the optimal positioning of the telescope and in the determination of the resolution of the new VELO detector. The efficiency as a function of bias voltage has to be understood precisely both to get the highest possible statistics for the study and for a safe characterisation of efficiency and noise of the new prototypes. Finally, the VELO simulation in the LHCb software can be checked and improved.

The detectors and experimental setup are summarised in section 2. Section 3 gives details of the clustering algorithm used in this study. The telescope alignment is discussed in section 4. In section 5 the efficiency determination is described. The principles of the track fit and resolution measurement are discussed in section 6. Section 7 describes the determination of the resolution as a function of angle, and in section 8, a measurement of capacitive charge sharing between adjacent strips is presented. In section 9, the results are compared with a Monte Carlo simulation of the silicon and with the simulation that is currently implemented in SICb. Section 10 summarizes the results.

2   The Detectors and Telescope Setup

The 1998 Hamamatsu detectors were made from 300 μm thick n-on-n wafers and are the first prototype for the LHCb VELO detector. The detectors have been described in detail in [1]. They are illustrated diagramatically in figure 1. The r type detectors have circular strips with pitches of 40μm and 60μm, and the ϕ-type detectors have the strips arranged radially, with pitches varying between 46μm and 126μm. Each strip in the ϕ-type detector is rotated by $5°$ about its centre to provide stereo information. The telescope detectors are equipped with VA2 [2] readout chips, whose performance is also described in [1].

The detectors were mounted in a telescope frame as illustrated in figure 2. The detector planes are all roughly parallel to each other, but angles of about $1°$ between the detector planes are typical. In order to take data with the tracks passing through the detectors at an angle the entire telescope was turned. In this way, only one set of alignment constants had to be determined with the telescope frame as reference. In order to be able to access the largest possible angle, while still having the track pass through all detector planes, the detectors were moved as close together as the mechanics allowed. In practice, the largest achievable angle was roughly 9 degrees.

3   Clustering Algorithm

A charged particle traversing a detector plane can produce a signal on one or several adjacent strips on the detector. Clusters were formed from the signals in the strips as follows:

1. The cluster formation begins with the strip on the detector that contains the largest signal. The signal over noise value of this strip is required to satisfy a cut typically set to $S/N > 15$.
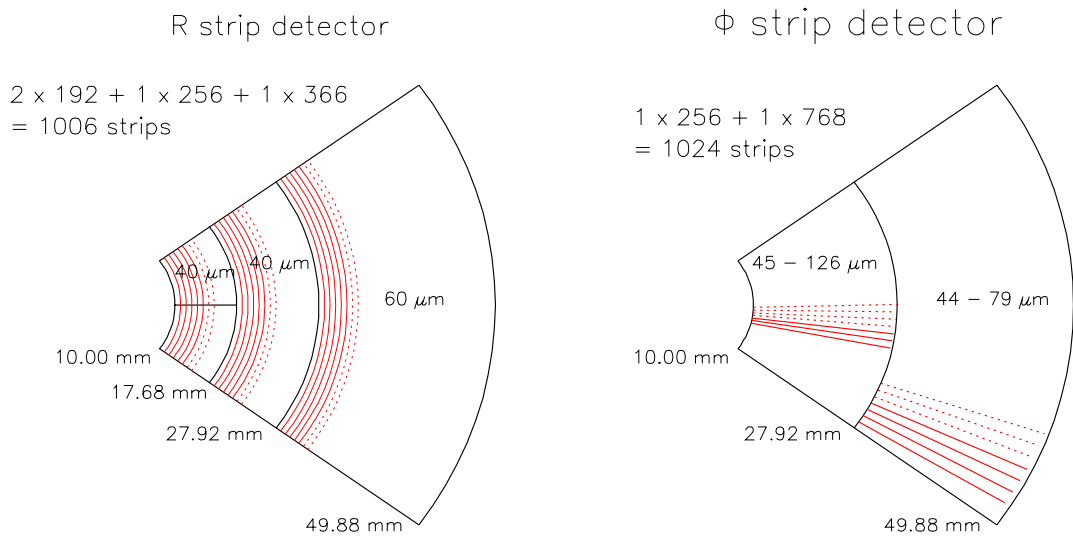
R strip detector

2 x 192 + 1 x 256 + 1 x 366
= 1006 strips

40 μm   40 μm

60 μm

10.00 mm

17.68 mm

27.92 mm

49.88 mm

Φ strip detector

1 x 256 + 1 x 768
= 1024 strips

45 − 126 μm

44 − 79 μm

10.00 mm

27.92 mm

49.88 mm

Figure 1: Diagrammatic layout of the strips on the VELO r and ϕ prototype detectors.

Dark box

7 cm

Scintillator triggers

2 3   5 4   6 7

Rϕ ϕR   Rϕ

Telescope support

Beam
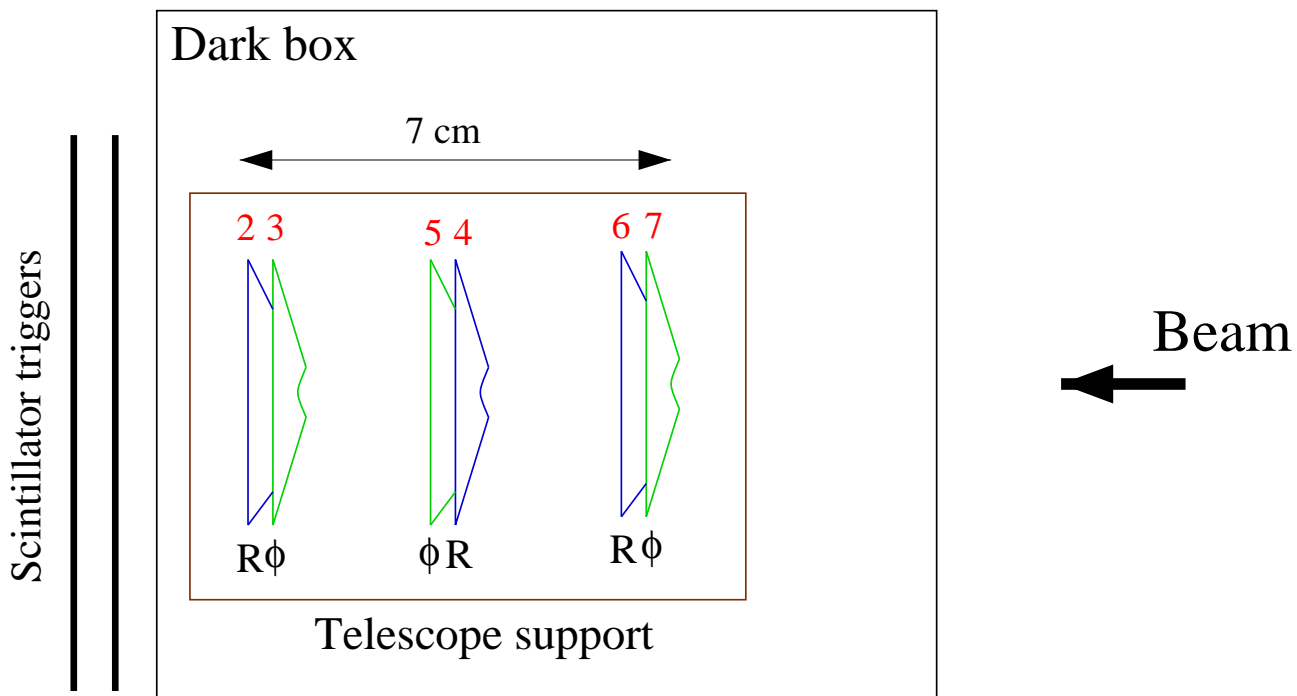
Figure 2: Diagrammatic layout of the detectors in the telescope frame. The numbers correspond to the detector numbering that is referred to in the text.

2

2. The neighbouring strips are added if they pass at least one of the following cuts:

   - The signal on the neighbouring strip passes the same signal over noise cut that was required for the first strip of the cluster (e.g. $S/N > 15$).
   - The signal in the neighbouring strip is larger than 10% of the signal in the first strip of the cluster (which contains the largest signal).

3. If a neighbouring strip was added on one side of the cluster, one more strip in that direction is also added if it passes at least one of the requirements listed above in step 2.

4. The next cluster is formed starting with the remaining strip with the highest signal on the detector.

5. Clusters are formed until all strips with signals satisfying the signal over noise cut are assigned to clusters.

The most probable value for cluster signal to noise is about 50. For the track angles considered in this analysis, the clusters usually contain no more than three strips. The cluster position is evaluated from the charge weighted average of the positions of the strip with the largest signal and its two immediate neighbours (if they belong to the cluster). The above clustering algorithm is robust, and the results do not depend on the exact value of the signal to noise cut (compare figure 10 with 18 and 14 with 19).

4 Alignment

As the telescope detectors were moved closer together, the z position was tracked with a micrometer to about 20μm precision. This information was used together with the alignment constants determined for the previous position [3] to start the alignment process. The telescope was aligned using approximately 30000 tracks split evenly among 4 different angles between 0 and 9 degrees. The alignment cannot determine the absolute z positions of the detectors, therefore the distance between detector 2 and detector 4 was kept constant during the alignment (see figure 2). The relative z positions of the r and ϕ detectors were also fixed by holding the distance between detector 2 and detector 3 constant to the original measured value. All other degrees of freedom of all detectors were allowed to vary.

The complete set of tracks were fitted through the telescope using the initial estimates for the alignment constants. A quantity χ^2 was computed for each detector by summing the squares of the residuals divided by the measurement error. For the measurement errors the approximation of $p/(1.5\sqrt{12})$ was used, where p denotes the strip pitch. The free parameters allowed for each detector were varied in MINUIT so as to minimise χ^2. The tracks were then refitted, and the procedure was repeated for a second iteration. A third iteration was performed, but after the second iteration the results were already found to be stable [1].

The quality of the alignment is illustrated in figures 3 and 4 which show the mean values and widths of the fitted residuals as a function of r and ϕ in the local detector frame. The scatter on the means can be seen to be at the level of $1\,\mu$m. The fitted widths give an impression of the resolution measured in the detectors for tracks at a mixture of angles. Assuming the detectors to be equally spaced and to have the same resolution, the widths of the residual distributions should be multiplied by $\sim \sqrt{6}$ for the outer detectors (indices 2, 3, 6, and 7) and by $\sim \sqrt{\frac{3}{2}}$ for

---

[1]The time taken for this alignment procedure was 6 hours in batch on the lxplus machines.

the detectors in the middle station (indices 4 and 5), in order to obtain the detector precision. An accurate determination of the precision as a function of angle, together with the derivation of these numbers, can be found in the following sections. Here we point out only the gross features: the r detector has a fairly constant precision of about $6\,\mu$m in the $40\,\mu$m region, and of about $8\,\mu$m in the $60\,\mu$m region, whereas in the ϕ detectors the precision varies very rapidly as a function of r due to the changing pitch, reaching about $38\,\mu$m at the junction between the innermost and outermost region, where the pitch is $126\,\mu$m.

5 Efficiency Measurement

The efficiency was measured by fitting a track in 5 out of the 6 detectors, extrapolating to the remaining detector, and looking for a cluster on that detector. Only clusters within 1 mm of the point of interception are considered.

As there are only two detectors measuring the same coordinate as the detector under study, events were selected with one hit only in both of these detectors. This avoids the possibility of forming wrong combinations. The signal to noise cut for this study was set to $S/N > 15$. The most probable value of the Landau observed in the detectors had a signal to noise of about 50.

Part of the observed inefficiency is due to dead and noisy channels. Figures 5 and 6 show that these occur in particular at chip boundaries (each VA2 chip reads out 128 channels). A large fraction of dead and noisy channels is therefore probably due to readout chip problems, which are currently not understood. In order to deconvolute this part, a possibility was added to cut out such channels. In figure 5 the noise after common mode correction of all channels in all detectors is shown. The cut was made by setting a ceiling of 1.4 times the mean noise in each chip. In order to cut out dead channels, the noise before common mode correction was used. Figure 6 shows this noise, and the channels falling below the cut, which was set at 1.1 ADC counts. In total, about 1 per cent of channels were eliminated by using these cuts.

The efficiency was measured for a range of bias voltages from 55 V to 100 V. At 60 V and below, the noise and consequently the number of channels rejected by the noise cut increase, as illustrated in figure 7.

The efficiency measured in the central r and ϕ detectors is illustrated in figures 8 and 9. The maximum efficiency is obtained when operating the detectors at at least 90 V bias. When accounting for noisy and dead channels, the efficiency is constant down to about 70 V bias, but the number of noisy and dead channels increases on the r detector below 90 V. Below 70 V, large inefficiencies are observed on both detectors. With decreasing bias voltage, these inefficiencies first appear on the r detector, and only in limited regions, see figure 8. The results suggest that this effect is due to variations in the silicon quality leading to somewhat different depletion voltages depending on the position on the wafer.

6 Principle of the Resolution Measurement

6.1 Clustering

In the track fit, the position of the clusters on the telescope detectors is given by the weighted mean of the strip positions, where the weight is determined according to the charge signal on each strip belonging to the cluster. The position resolution of a cluster on a telescope detector depends on the number of strips in the cluster. For clusters with two or three strips, the
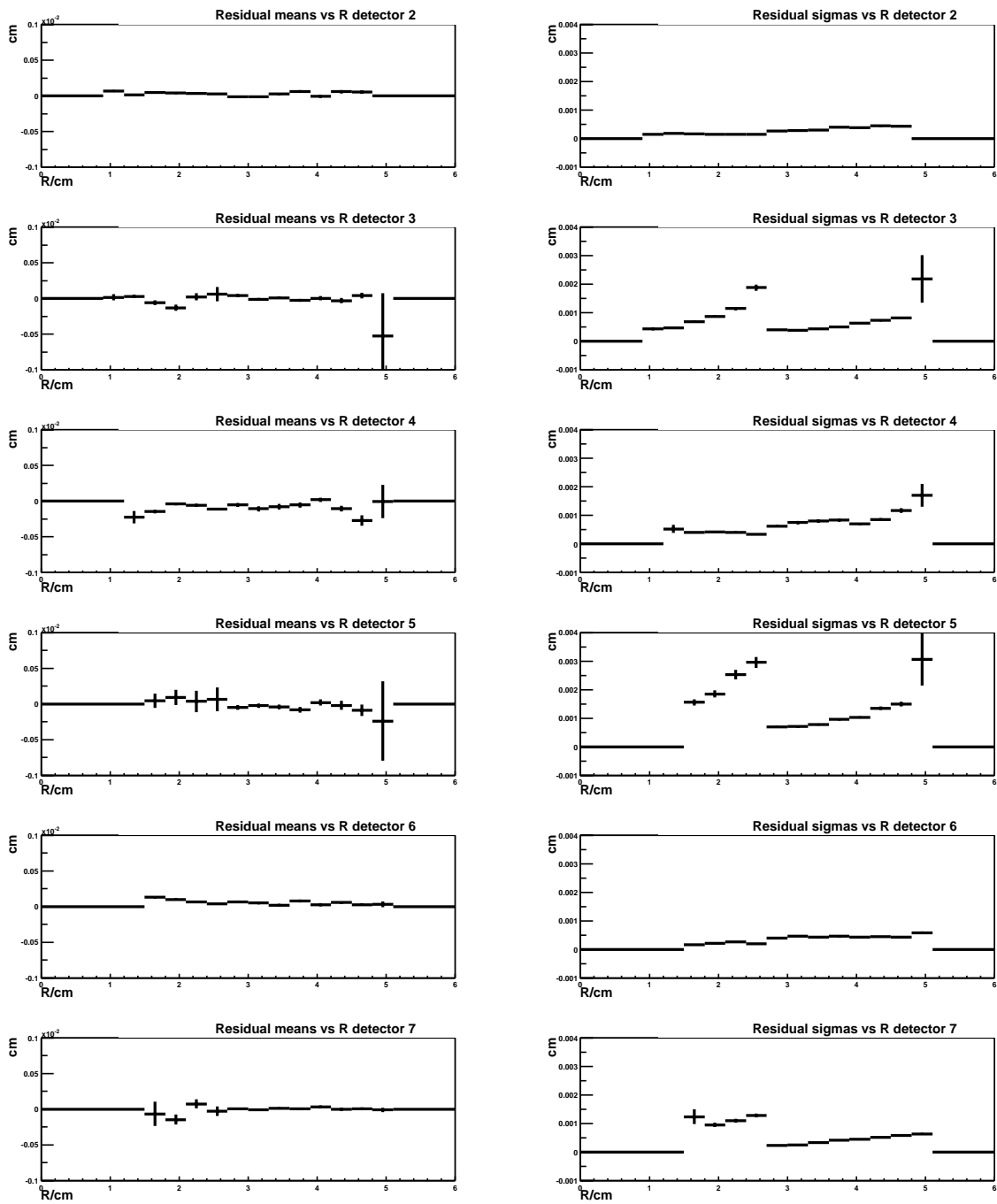
Figure 3: The mean values (left column) and widths (right column) of the residuals as a function of the radius on the detector. The two distributions in one row correspond to one detector. Detectors with even indices are r detectors, uneven indices correspond to ϕ detectors. Detectors 4 and 5 belong to the middle telescope station.
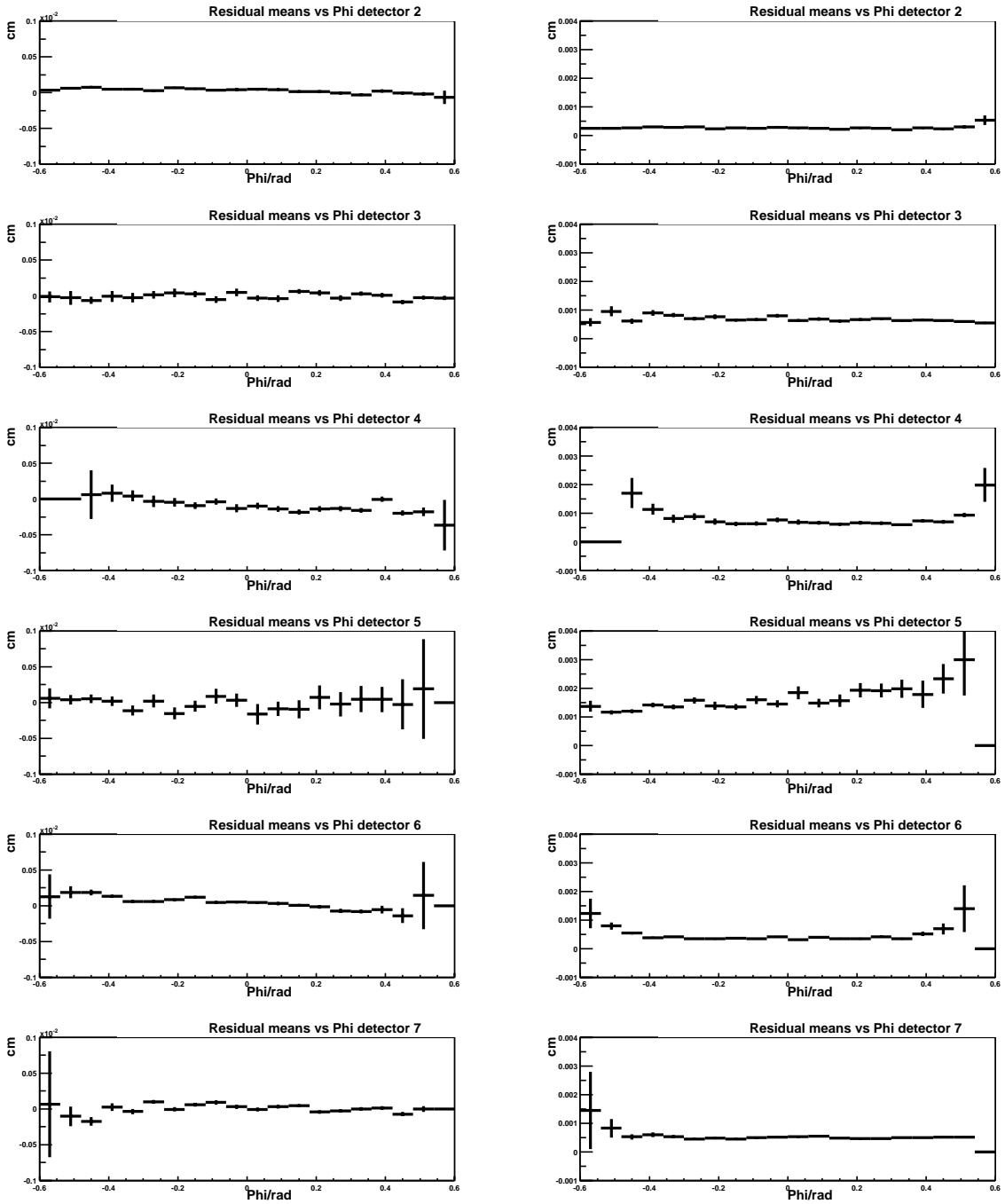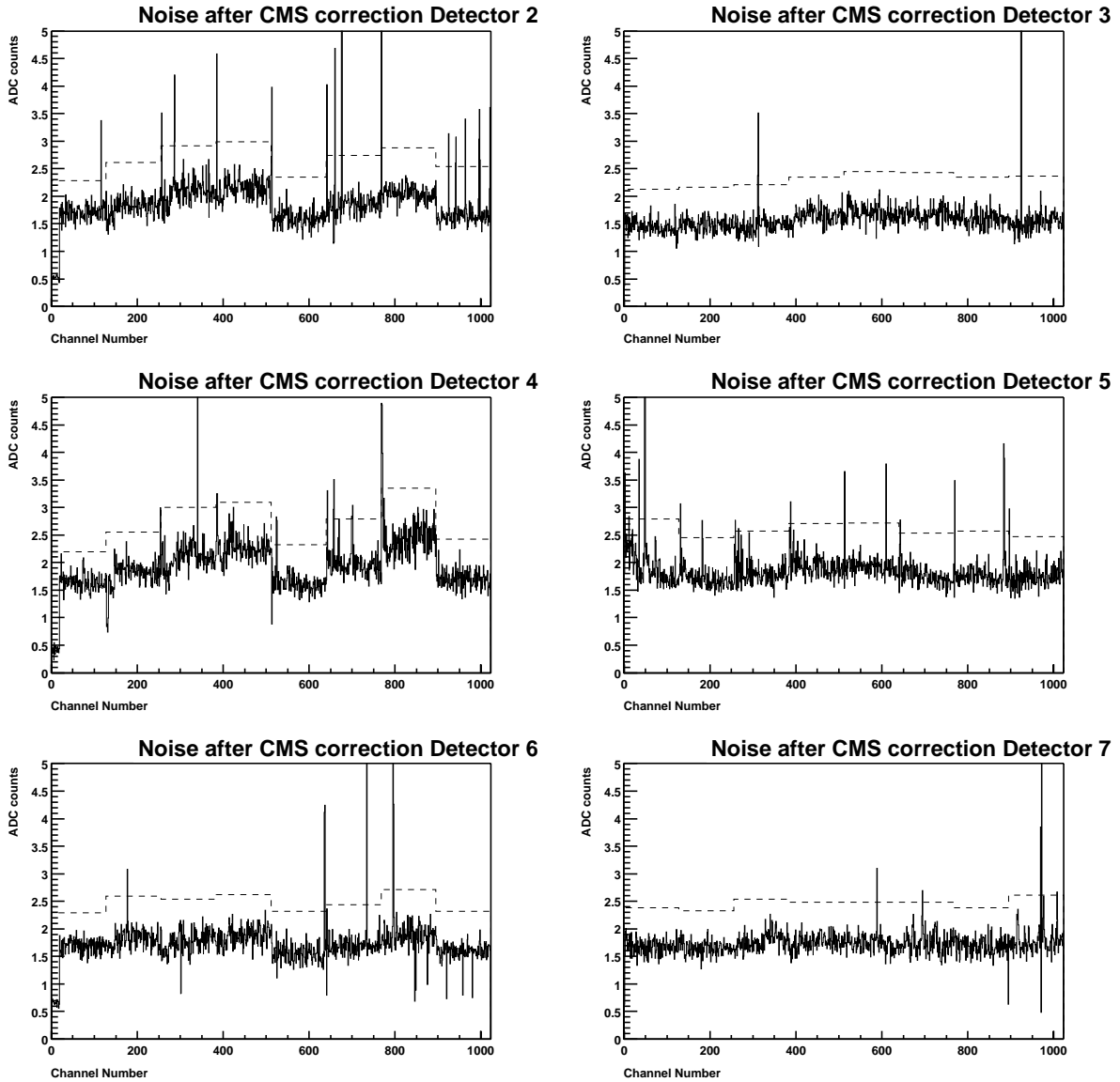
Figure 4: The mean values (left column) and widths (right column) of the residuals as a function of ϕ on the detector. The two distributions in one row correspond to one detector. Detectors with even indices are r detectors, uneven indices correspond to ϕ detectors. Detectors 4 and 5 belong to the middle telescope station.

Figure 5: The noise after common mode correction on each of the six telescope detectors. The left column shows r detectors, while the noise for ϕ detectors is given on the right. The dashed line indicates the ceiling at 1.4 times the noise in each chip, to identify noisy channels. The first channels in the r detectors are not bonded.
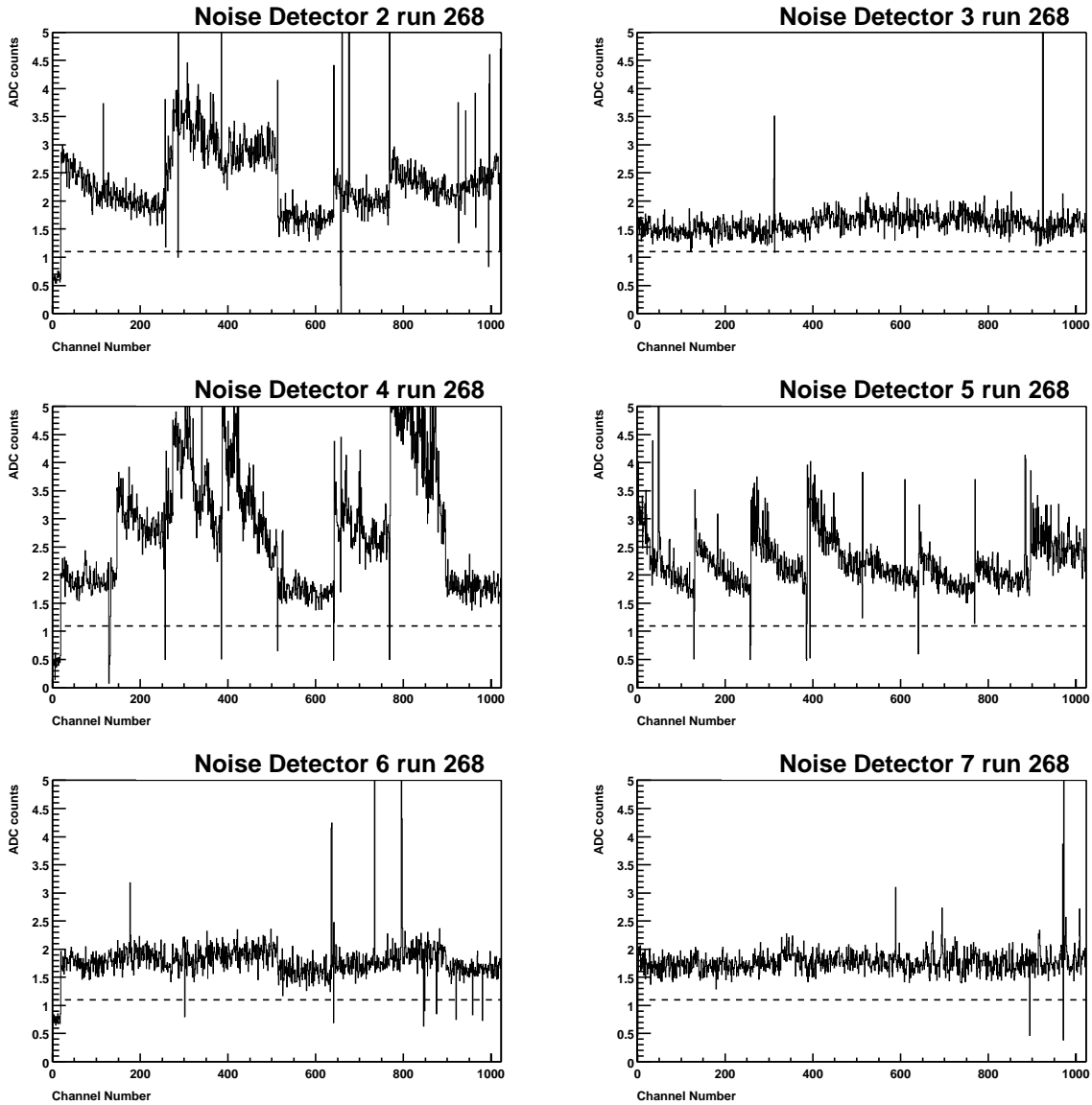
Figure 6: The noise before common mode correction on each of the six telescope detectors. The left column shows r detectors, while the noise for ϕ detectors is given on the right. The dashed line indicates the cut at 1.1 ADC counts, which is applied to identify dead channels. It is instructive to compare the noise before common mode correction of the dead channels with that of the first 18 channels on the r detectors, which were not bonded.
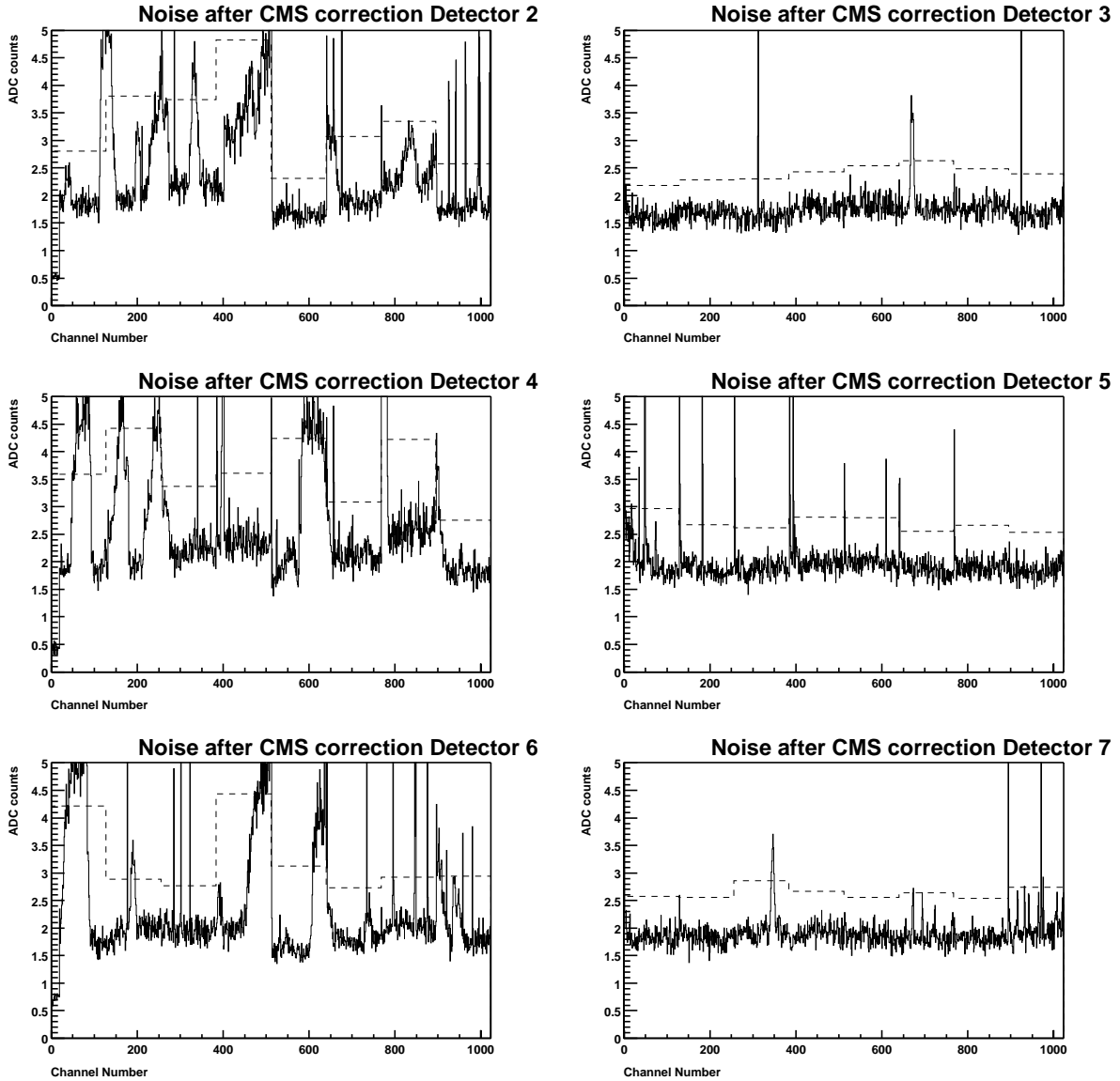
Figure 7: The noise after common mode correction on each of the six telescope detectors. In this run, the detectors were operated at only 60V bias. A significant increase in noisy channels is observed.
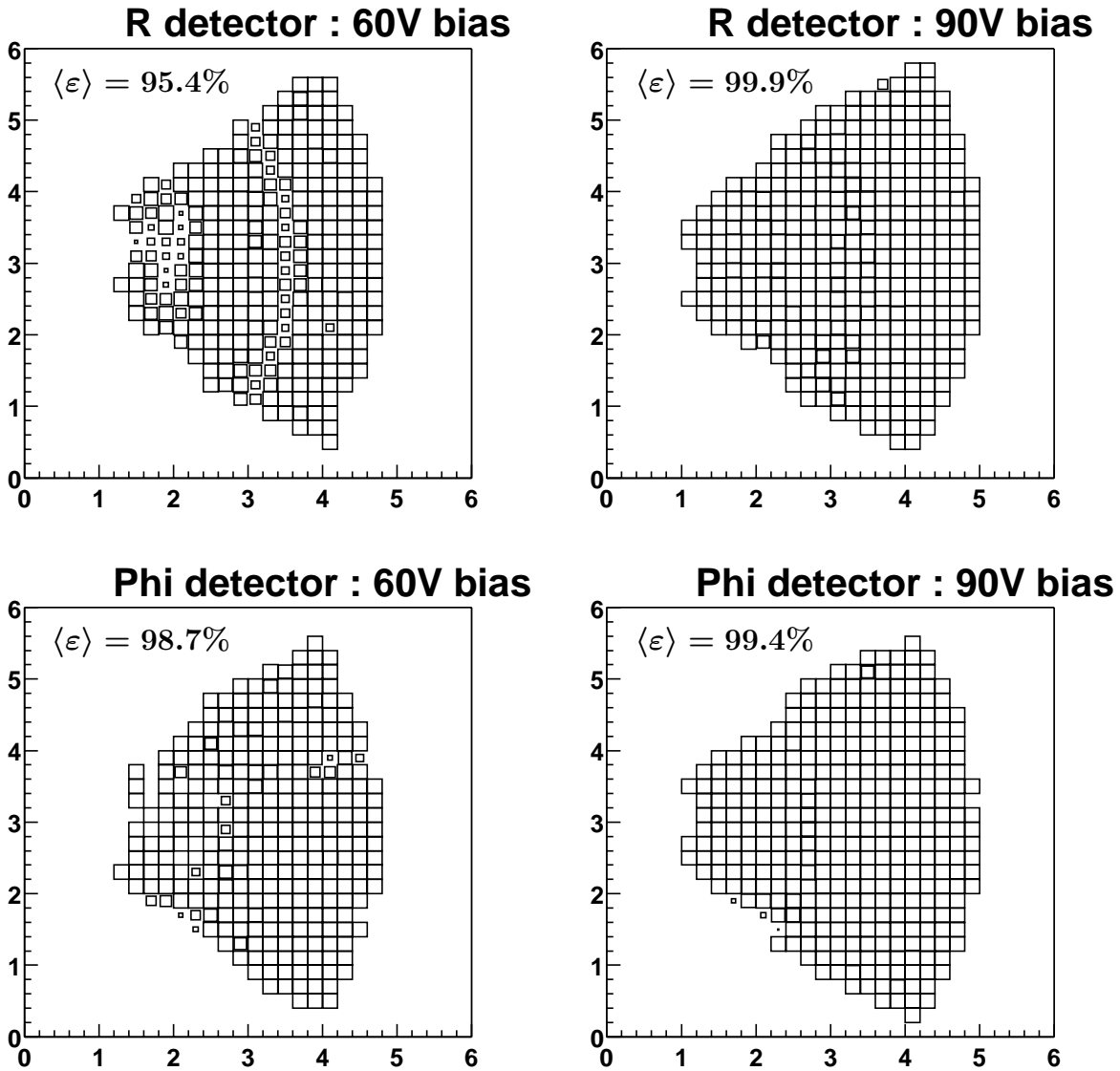
9

Figure 8: The cluster finding efficiency as measured on the central r and ϕ detectors for 60 V and 90 V bias. On each plot, the horizontal and vertical axes indicate the local coordinates on the detector in cm, while the area of the boxes in the histogram is proportional to the efficiency at a given location (a full box corresponds to 100% efficiency). The mean efficiencies (integrated over the detector area) after accounting for dead and noisy channels are indicated in the plots.
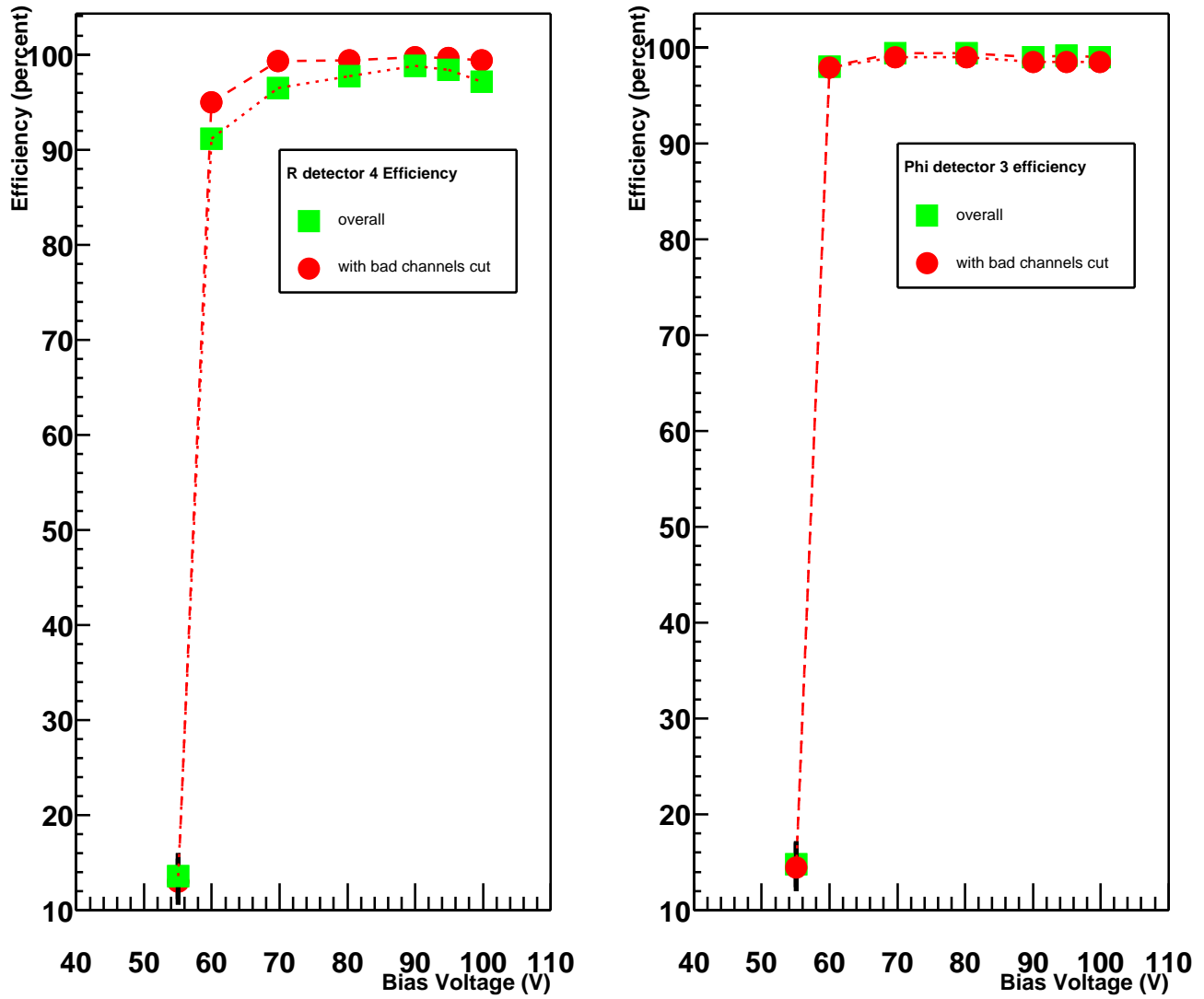
Figure 9: The cluster finding efficiency as a function of bias voltage for r and ϕ detectors. In each case, the green squares indicate the overall efficiency, while for the red points, clusters containing dead or noisy strips are not considered in order to separate the direct dependence on the bias voltage.

weighting improves the cluster position. For large numbers of strips, the signal over noise level on individual strips may drop below threshold, and the resolution is expected to deteriorate.

The average position resolution of a silicon detector is then a function of the angle α of incidence of the particle: The charge is collected perpendicular to the detector plane, and with increasing angles, the average number of strips per cluster also increases. More precisely, the relevant parameter is l_p/p, the distance l_p perpendicular to the strips between the entry and exit points of the particle when traversing the detector, normalised to the strip pitch p. The following study is therefore based on the *projected angle* α_p, which is defined by

$$\tan \alpha_p = \frac{l_p}{d} \ , \tag{1}$$

where d is the detector thickness. In figure 10, the fraction of clusters with a given number of strips is shown as a function of the projected angle.

For two-strip clusters, the distribution of the signal fraction in the strip with smaller signal is shown in figure 11 as a function of projected angle.

6.2 Track Fit and Resolution Measurement

The following is a simplified discussion of the track fit concerning a situation where the strips on all detectors are parallel, as in the resolution measurement. For the determination of alignment constants (see section 4) and in the efficiency study (cf. section 5), a more complicated fit in three dimensions was used which takes into account all rotations in the alignment constants as well as the stereo angles of the strips on the ϕ detectors.

For parallel strips, detectors spaced at positions z_i ($1 \leq i \leq n$), and measured cluster positions y_i ($1 \leq i \leq n$) on the detectors, a straight line fit given by

$$y = mz + c \tag{2}$$

yields [4]

$$m = \frac{\overline{yz} - \overline{y}\,\overline{z}}{\overline{z^2} - \overline{z}^2} \quad \text{and} \tag{3}$$

$$c = \overline{y} - m\overline{z} \ , \tag{4}$$

where the symbol $\overline{x}$ denotes the weighted average of a quantity x, i.e.

$$\overline{x} = \frac{1}{\sum\limits_{i=1}^{n} \frac{1}{\sigma_{x_i}^2}} \sum_{i=1}^{n} \frac{x_i}{\sigma_{x_i}^2} \ . \tag{5}$$

The residual

$$\Delta y_i = y_i - (mz_i + c) \tag{6}$$

of a cluster on detector i with respect to the track is defined as the distance between the weighted cluster position and the point where the track crosses the detector plane. Given the spacing of the detectors in z and their relative resolution, it is possible to relate the width of the distribution of residuals on one of the detectors to this detector's resolution (even if the information from the detector under consideration is used in the track fit). The error on the residual on detector k is given by

$$\sigma_{\Delta y_k} = \sqrt{\sum_{i=1}^{n} \left(\frac{\partial \Delta y_k}{\partial y_i} \sigma_{y_i} \right)^2} \ , \tag{7}$$
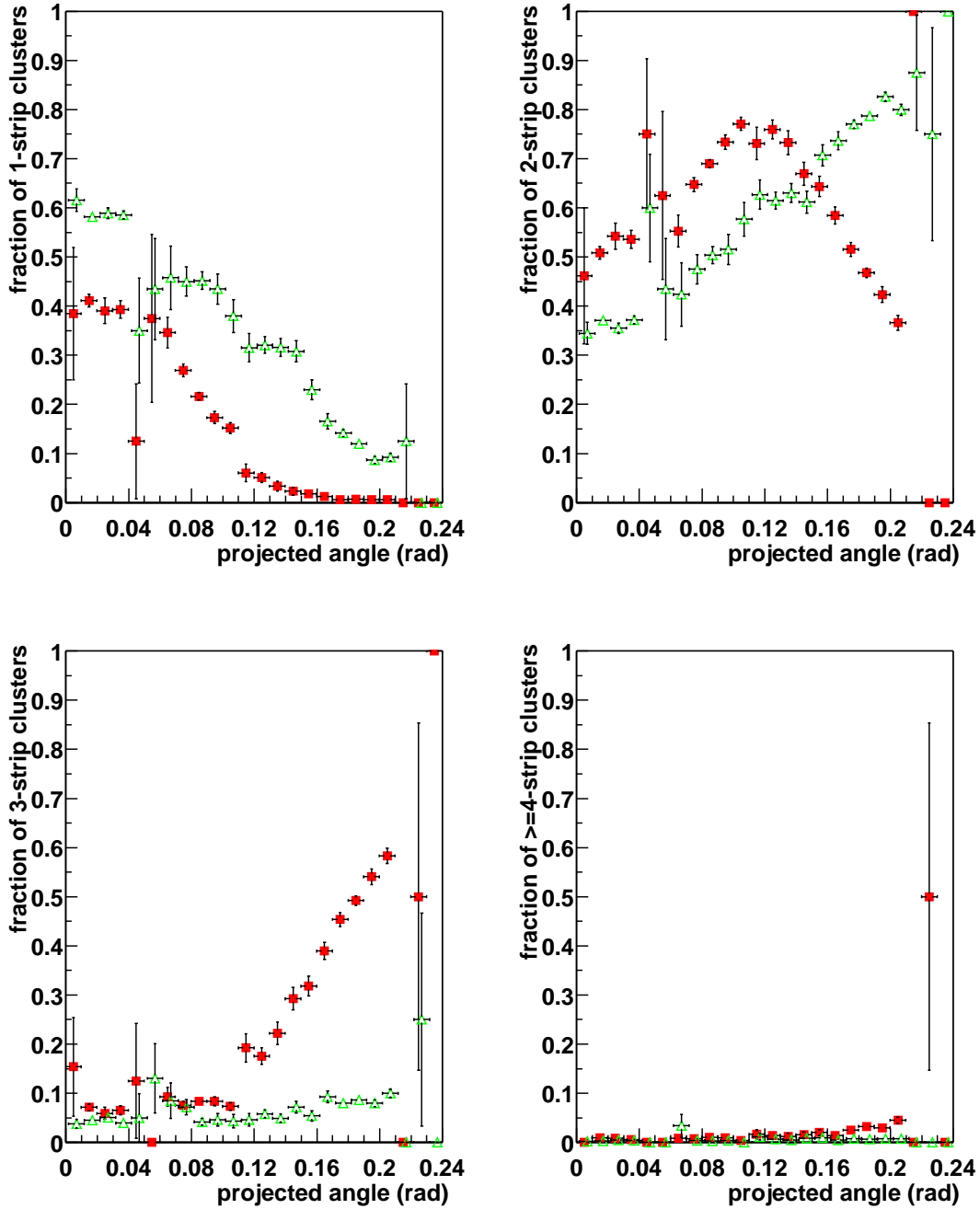
12

Figure 10: The fraction of clusters with a given number of strips as a function of the projected angle of the incident particle. The solid red squares denote the measurement in the $40\,\mu$m pitch region on a $300\,\mu$m thick detector, and the open green triangles correspond to the $60\,\mu$m pitch region.
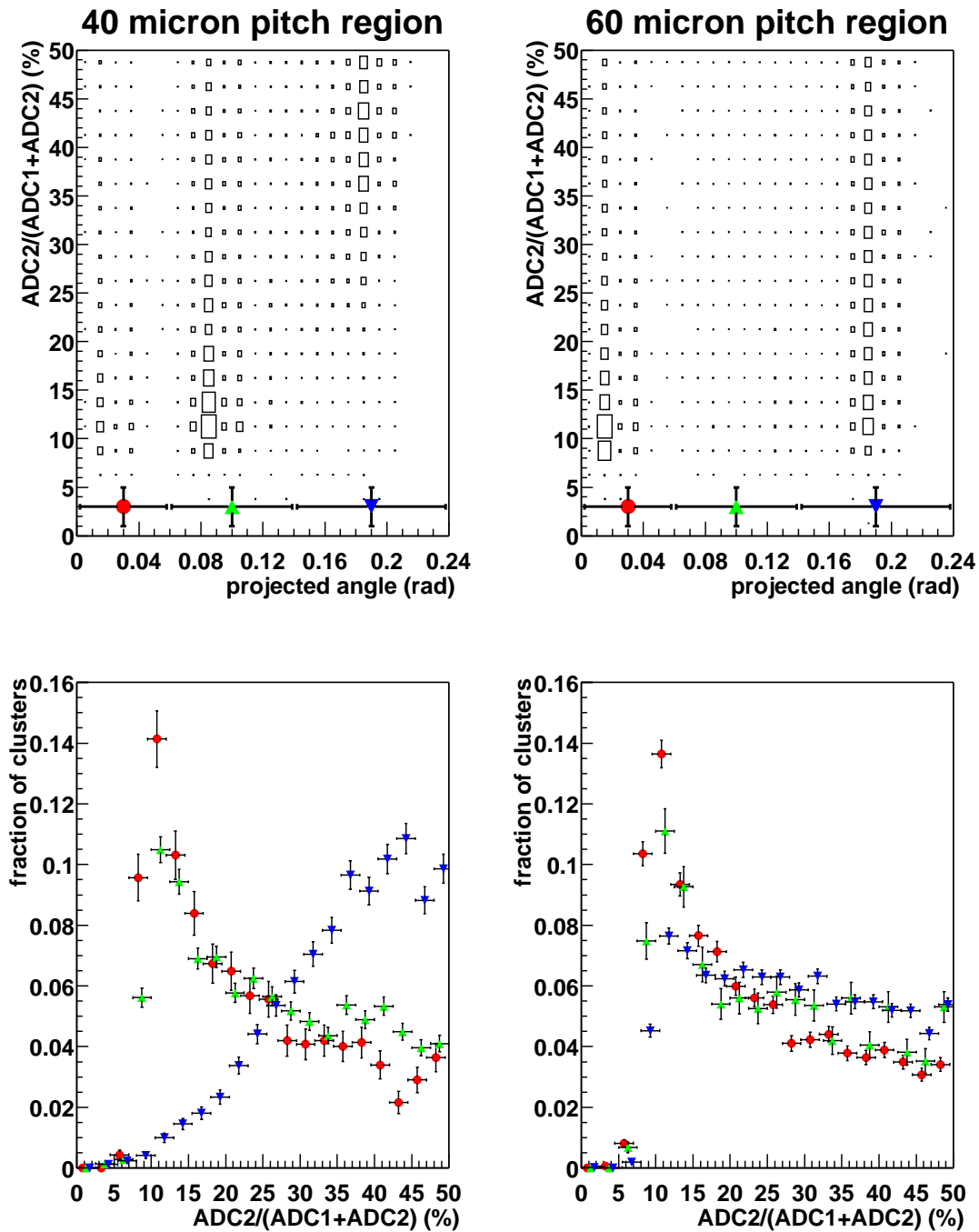
Figure 11: The signal fraction in the strip with smaller signal for clusters containing two strips is shown for regions with $40\,\mu$m and $60\,\mu$m pitch. In the upper plots, the signal fraction is shown versus the projected angle of the track. In the lower histograms, the distribution of signal fractions is given for three ranges in projected angle as indicated in the upper plots.

where σ_{y_i} denotes the resolution of detector i, and

$$\frac{\partial \Delta y_k}{\partial y_i} = \delta_{ik} - \left(\frac{\partial m}{\partial y_i} z_k + \frac{\partial c}{\partial y_i} \right) \, . \tag{8}$$

Further,

$$\frac{\partial m}{\partial y_i} = \frac{1}{\overline{z^2} - \overline{z}^2} \left(\frac{\partial (\overline{yz})}{\partial y_i} - \frac{\partial \overline{y}}{\partial y_i} \overline{z} \right) \tag{9}$$

and

$$\frac{\partial c}{\partial y_i} = \frac{\partial \overline{y}}{\partial y_i} - \frac{\partial m}{\partial y_i} \overline{z} \, . \tag{10}$$

In the following, it is assumed that the detector z positions are known with "equal and infinite" precision, while the resolution on the individual detectors may vary. Then,

$$\frac{\partial \overline{y}}{\partial y_k} = \frac{1}{\sigma_{y_k}^2 \sum\limits_{i=1}^{n} \frac{1}{\sigma_{y_i}^2}} \quad \text{and} \tag{11}$$

$$\frac{\partial (\overline{yz})}{\partial y_k} = \frac{z_k}{\sigma_{y_k}^2 \sum\limits_{i=1}^{n} \frac{1}{\sigma_{y_i}^2}} \, . \tag{12}$$

A special configuration is the case of three silicon detector with equal spacing and equal resolution. In this case, one finds (see the appendix for a derivation)

$$\sigma_{\Delta y_{\text{outer}}} = \sqrt{\frac{1}{6}} \sigma_y \quad \text{and} \tag{13}$$

$$\sigma_{\Delta y_{\text{middle}}} = \sqrt{\frac{2}{3}} \sigma_y \tag{14}$$

for the two outer and the middle detector, respectively.

In general, the relative z positions of the detectors have to be determined from the alignment procedure. The resolution on the detectors are generally not identical, but may vary because of different strip pitches, but also if the detectors are at slightly different (projected) angles with respect to the incident particles.

6.3 Track Fit and Extrapolation Precision

A similar problem is the case where the extrapolation precision of a track has to be determined for the z position of a detector that has not been used in the track fit. Starting from equation 2, the extrapolation precision at a position z is given by

$$\Delta y = \sqrt{\sum_i \left(\frac{\partial y}{\partial y_i} \sigma_{y_i} \right)^2} \, , \tag{15}$$

where the y_i denote the measurements on the detectors used in the track fit, as before. From equations 9 and 10, one then has

$$\frac{\partial y}{\partial y_i} = \frac{\partial m}{\partial y_i} z + \frac{\partial c}{\partial y_i}$$

15

$$= \frac{1}{\overline{z^2} - \overline{z}^2} \left(\frac{\partial(\overline{yz})}{\partial y_i} - \frac{\partial \overline{y}}{\partial y_i} \overline{z} \right) (z - \overline{z}) + \frac{\partial \overline{y}}{\partial y_i}$$

$$= \left(\frac{(z - \overline{z})(z_i - \overline{z})}{\overline{z^2} - \overline{z}^2} + 1 \right) \frac{1}{\sigma_{y_i}^2 \sum_j \frac{1}{\sigma_{y_j}^2}} \quad . \tag{16}$$

One can see that the best extrapolation precision is achieved at the weighted centre of all measurements, i.e. at $z = \overline{z}$, where

$$\Delta y(z = \overline{z}) = \frac{1}{\sum_j \frac{1}{\sigma_{y_j}^2}} \sqrt{\sum_i \left(\frac{1}{\sigma_{y_i}^2} \sigma_{y_i} \right)^2} = \frac{1}{\sqrt{\sum_i \frac{1}{\sigma_{y_i}^2}}} \quad . \tag{17}$$

For equal resolution on all detectors, this formula simplyfies further to

$$\Delta y(z = \overline{z}, \text{ equal resolution}) = \frac{\sigma_y}{\sqrt{n}} \quad . \tag{18}$$

In summary, if $z = \overline{z}$, the extrapolation precision is the same as if all detectors were measuring at the same point in z.

7 Determination of the Resolution as a Function of Projected Angle

As outlined in section 6.1, the average resolution of a silicon strip detector will have a minimum at a projected angle of incidence of the particles which is different from zero (so that the fraction of one-strip clusters is small) but not too large (to ensure a small fraction of clusters with large strip number). The determination of the resolution as a function of projected angle is discussed in this section.

Note that the resolution can be inferred from the residual distribution on any detector. In the testbeam setup, there are three r detectors, while there are two parameters to be determined for each track. Since there is only one degree of freedom, only the information from one detector (called the *selected detector* in the following) can be used to obtain the resolution as a function of projected angle (in the track fit, all detectors are of course used). As a cross-check, the same dependence should be obtained no matter which detector is selected.

Following the discussion in section 6, the resolution of a detector can be determined only

- if the relative z positions of the detectors are known and

- if the relative detector resolutions are known.

The z positions are assumed to be known from the alignment. In order to take into account the relative detector resolutions for each track, an iterative procedure is needed:

1. In a first iteration, it is assumed that the resolution is the same on each of the detectors. It is assumed that the resolution depend on the projected angle α_p as

$$\sigma(y) = \frac{a}{\alpha_p^2 + b} + c\alpha_p \quad , \tag{19}$$

where the parameters a, $b > 0$, and c are to be determined. The particular functional form is not important; however, the function is needed for interpolation during the iteration. Only tracks for which all clusters on the r detectors lie in the region with $40\,\mu$m strip pitch are selected.

2. For each track, the projected angles of incidence on each of the detectors are determined, accounting for the alignment constants. The distribution of projected angles are shown in figure 12 for tracks that pass entirely through the regions with $40\,\mu$m or $60\,\mu$m pitch. The structure in the plots is explained as follows:

   - Since the r strips are not straight, detectors with a given inclination α around an axis parallel to the r strips in the centre of the detector yield a distribution of projected angles α_p that peaks at $\alpha_p = \alpha$ but has a tail towards lower values from tracks that pass the detector at the edges of the r strips.

   - The radius (local radial coordinate on the detector) at which the particles passed the detectors increases from the detectors shown in the top row of figure 12 to those in the bottom row. Since the tracks are parallel (the beam spot size is the same on all detectors), the spread in the α_p distribution diminishes from top to bottom.

3. The resolutions on each of the detectors are obtained from the currently assumed dependence of the resolution on the projected angle (equation 19). The track parameters are then computed as described in section 6.2 (disregarding the information from the ϕ detectors which in principle adds slightly to the r measurement because of the stereo angle).

4. The distribution of residuals versus projected angle is shown in figure 13. In each bin of the projected angle of the incident track, the width of the distribution of the residuals on the selected detector is determined from a Gaussian fit.

5. With the assumed resolutions on each detector, the residual widths on the selected detector are converted into the corresponding resolution for each bin in projected angle according to equations 7 to 12.

6. The function in equation 19 is fitted to the resolution as a function of projected angle. This is necessary because data have not been taken for all projected angles (see figure 12). On the other hand, because of non-zero angles between the detectors, the projected angles are different for the three detectors. To determine the resolution on each of the detectors, an interpolation between the measurement points is necessary in each iteration, which is provided by the fitted function.

   In figure 14, the measurements of the resolution as a function of projected angle are shown for all iterations. The fitted functions are also given.

7. The procedure is repeated starting at 3. until the resolution as a function of projected angle is stable. It has been checked that after the fourth iteration, any changes in the resolution as a function of projected angle are negligible.

The iterative procedure is used for all detectors as "selected" detectors in turn. In addition to the tracks passing through the region with $40\,\mu$m pitch, the study is also done for tracks formed of clusters that are all in the region of $60\,\mu$m pitch. The results from the final iteration are compared in figure 15. Reasonable agreement between the results from the different detectors is observed. Note that the information from the different detectors is not independent, as discussed above.

It was tested whether the fluctuations in the measured resolution could be due to effects like misalignment which could cause a dependence of the measured resolution on the angle ϕ
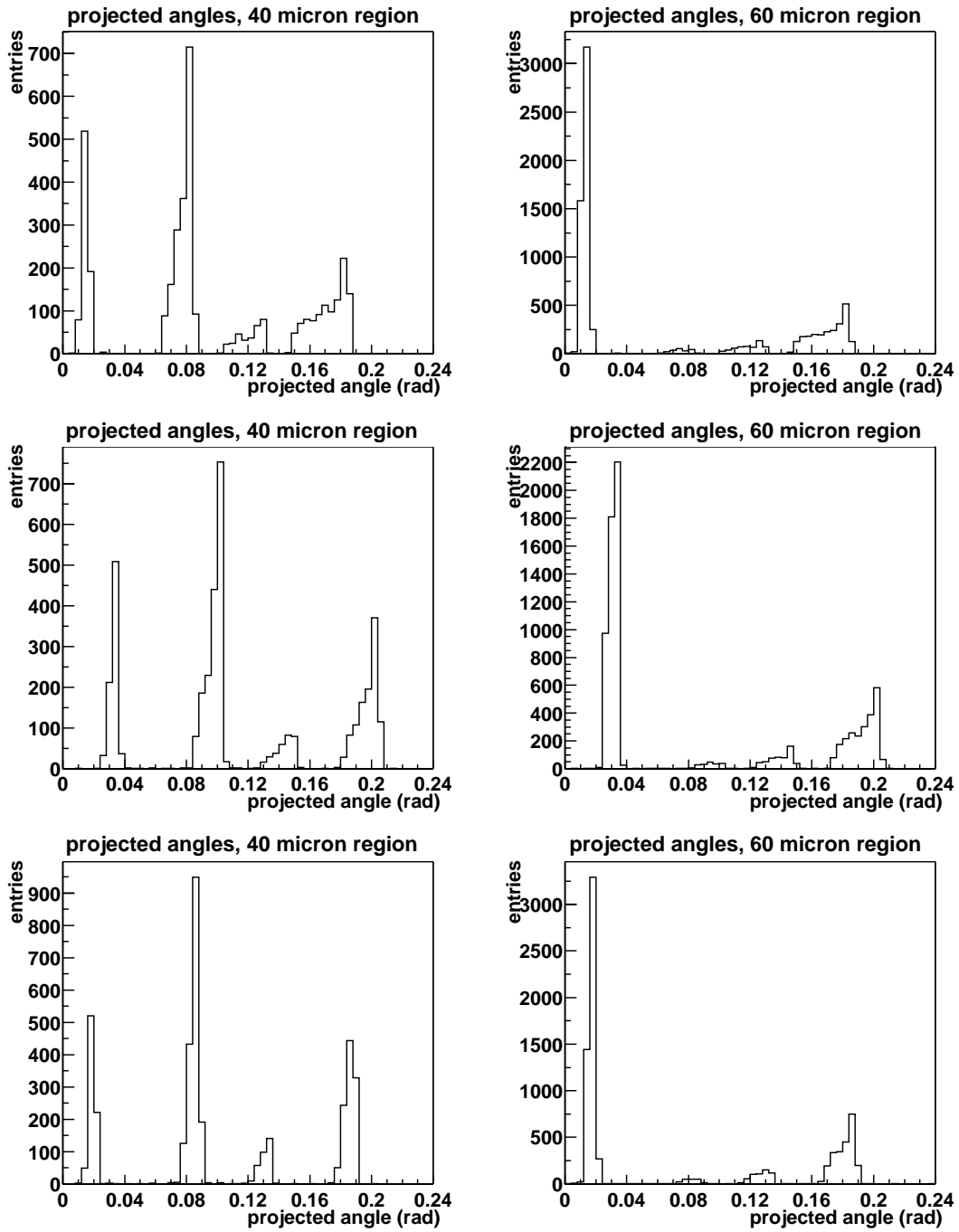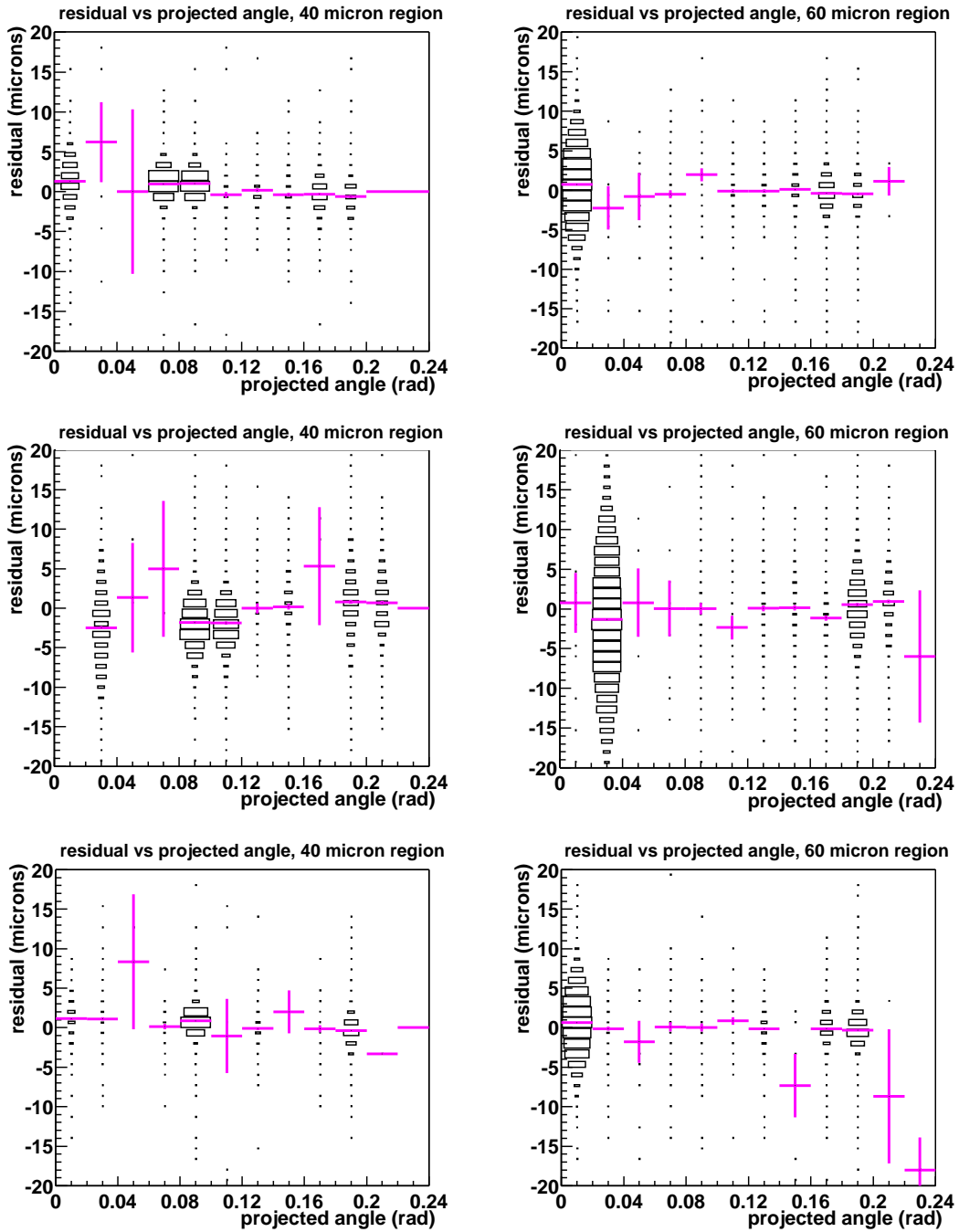
Figure 12: The distribution of projected angles on the three r detectors. Each row gives the distribution on one detector. The left column shows tracks passing through the $40\,\mu$m pitch region on all three r detectors. Tracks passing through the $60\,\mu$m pitch regions are shown on the right.

Figure 13: The distribution of residuals vs projected angles on the three r detectors. Each row gives the distribution on one detector. The left column shows tracks passing through the 40 μm pitch region on all three r detectors. Tracks passing through the 60 μm pitch regions are shown on the right. In each plot, the mean residuals as a function of track angle are superimposed as the pink histogram. For the plots shown here, the track parameters have been determined assuming the same resolution on all telescope detectors.

19
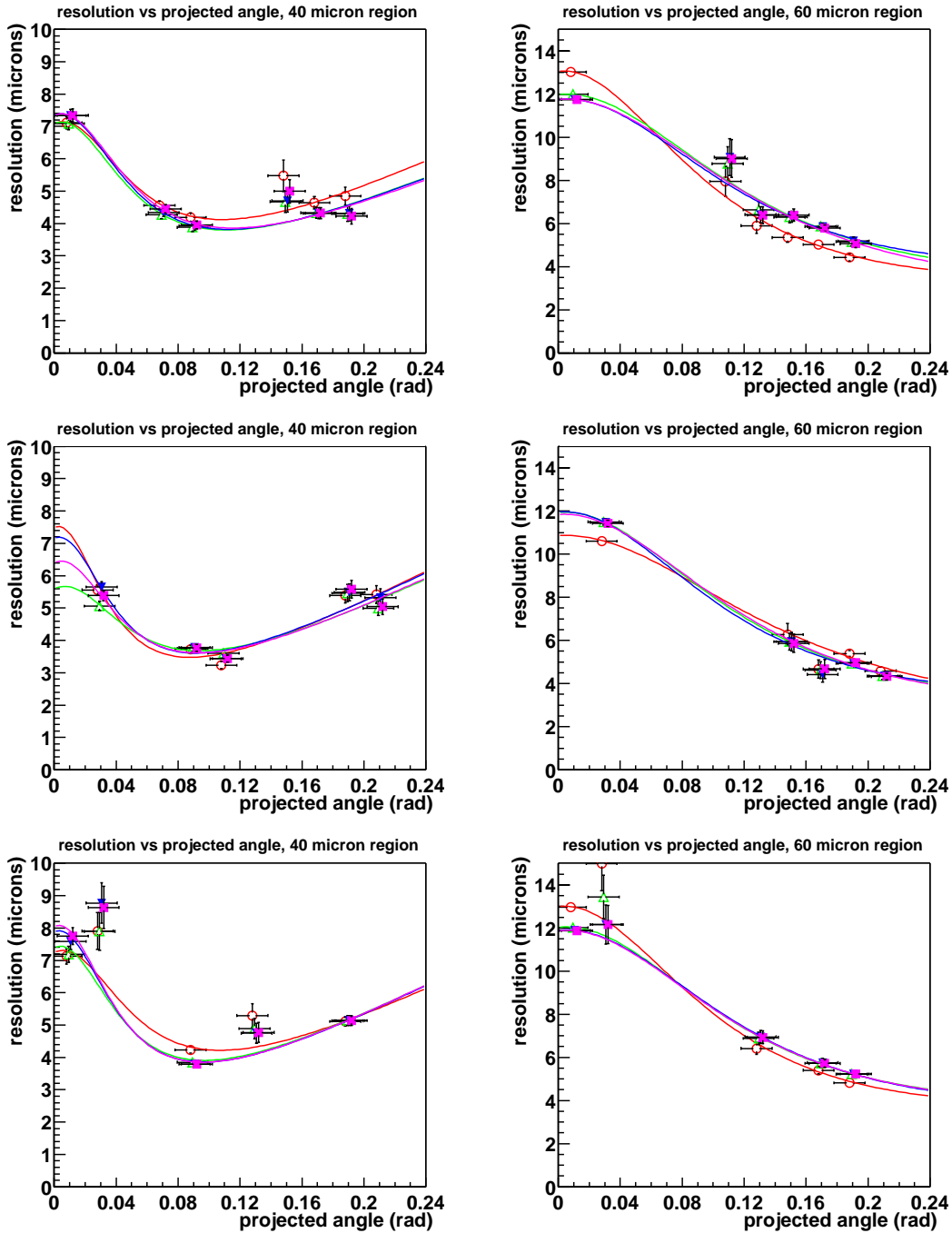
Figure 14: The resolution vs. projected angle on the three r detectors, corresponding to the three rows. The left and right columns show the results for the $40\,\mu$m and $60\,\mu$m pitch regions, respectively. The points with error bars denote the measured resolution, with red circles, green triangles, blue triangles, and pink squares corresponding to the first to fourth iteration, respectively. The points have been slightly offset horizontally for better visibility. The fitted resolution as a function of projected angle is shown for each iteration in the corresponding colour.
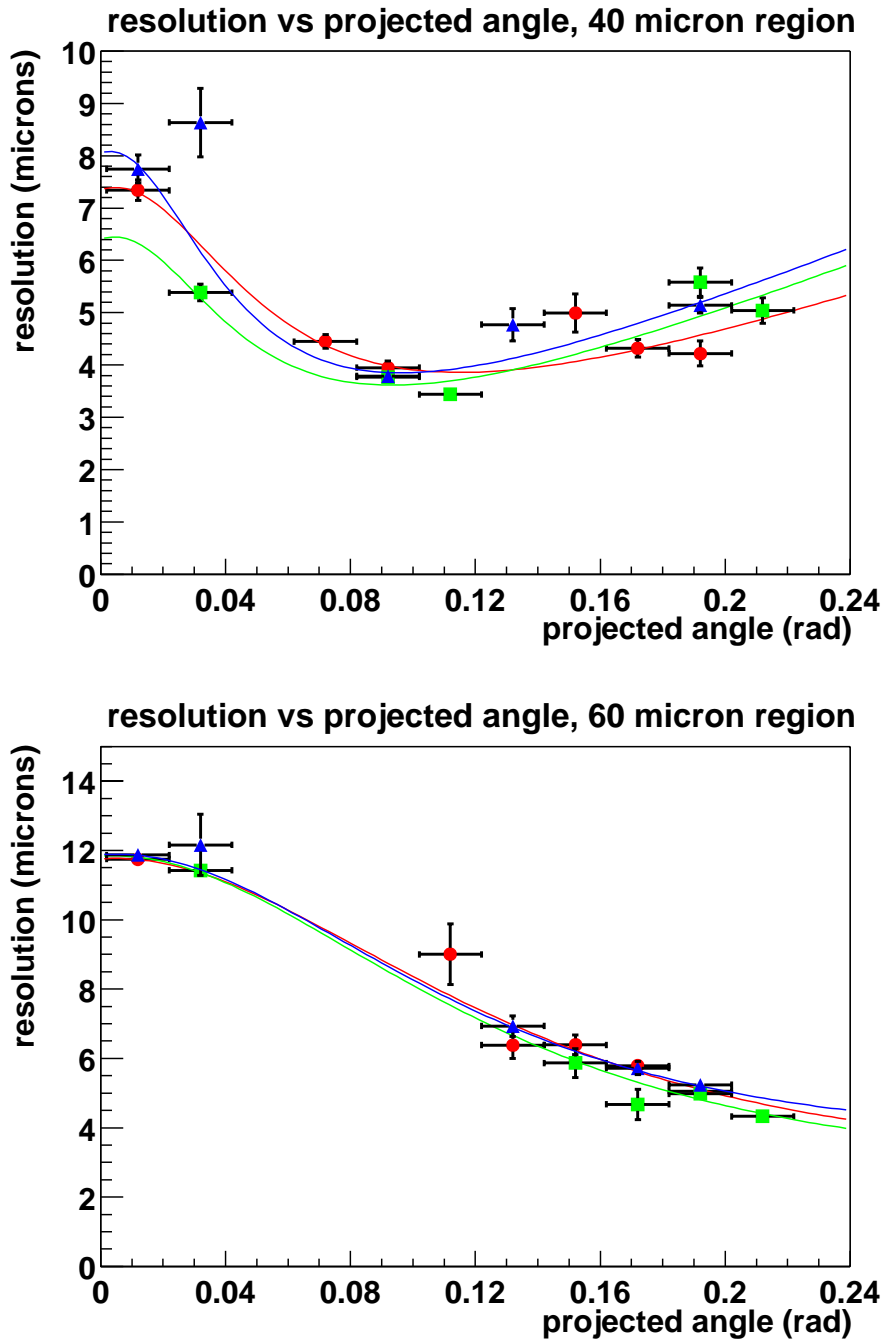
Figure 15: The resolution as a function of projected angle for the $40\,\mu$m and $60\,\mu$m pitch regions. The results for all three detectors are shown superimposed. Note that the information from the three detectors is not independent.

of the tracks. The procedure has therefore been repeated seperately for tracks passing through the upper ($\phi > 0$) and lower ($\phi < 0$) halves of the telescope detector. In general, the agreement is good, see figure 16. Significant differences are obtained for two measurement points in the $40\,\mu$m region, but no systematic deviation between the results is visible.
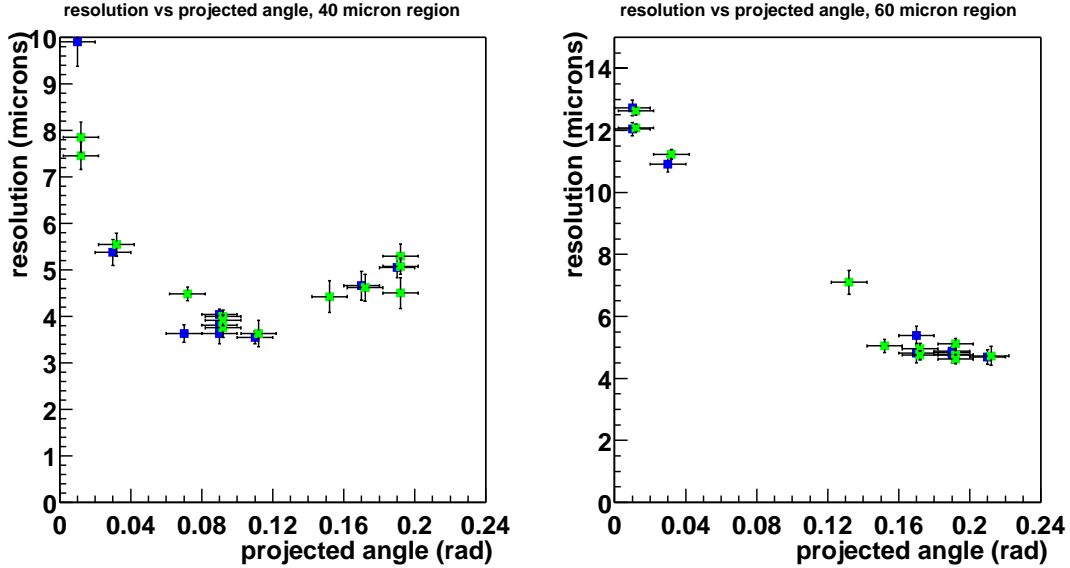
Figure 16: The resolution as a function of projected angle for the $40\,\mu$m and $60\,\mu$m pitch regions. Measurements with tracks passing through the region $\phi > 0$ are shown in blue, those in the region $\phi < 0$ in green.

The following best resolutions are obtained:

strip pitch	projected angle	resolution
$40\,\mu$m	$80 - 120$ mrad	$3.6 - 3.9\,\mu$m
$60\,\mu$m	≥ 200 mrad	$4.0 - 4.6\,\mu$m

The results are used in order to verify an improved simulation of the resolution in the VELO, as described in section 9. In the future, the simulation can then in turn be taken to optimise VELO parameters such as detector thickness and strip pitch in view of the resolution as a function of track angle. A qualitative study relating the geometrical impact parameter resolution and the single hit resolution as a function of track angle in LHCb is given in section 9.4.

7.1 Resolution for Different Cluster Sizes

For the modelling of the cluster resolution in the LHCb Monte Carlo simulation, it is important to know whether there is a significant dependence on the projected angle for a given fixed cluster size.

The study is therefore repeated with tracks that contain only one-strip clusters, two-strip clusters, and clusters with three or more strips. The results are shown in figure 17. Because of the requirement of a fixed cluster size for all three clusters, the available statistics are limited to small (large) projected angles for one-strip (three-strip or larger) clusters (see also figure 10).
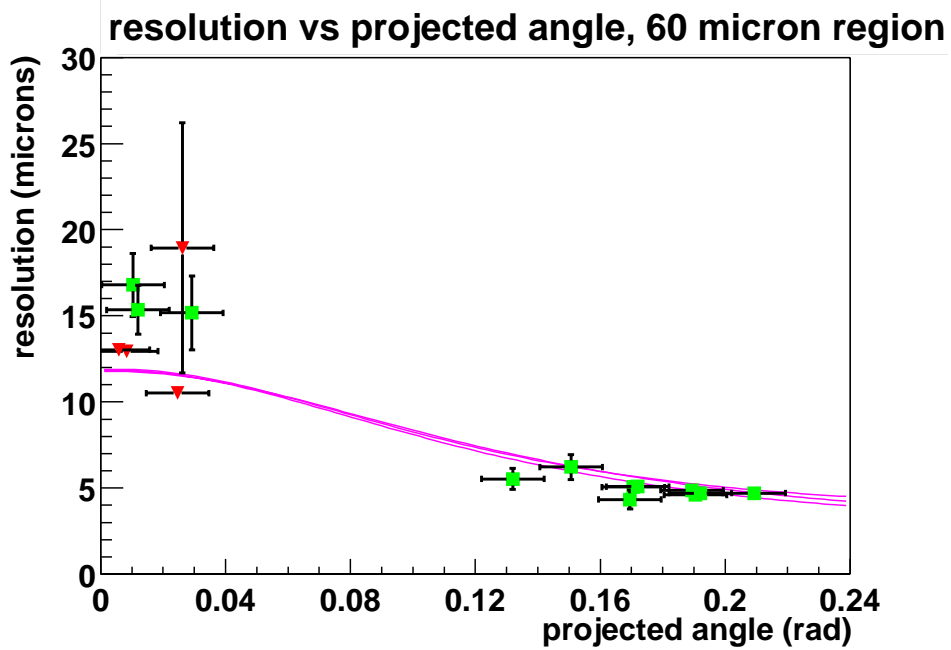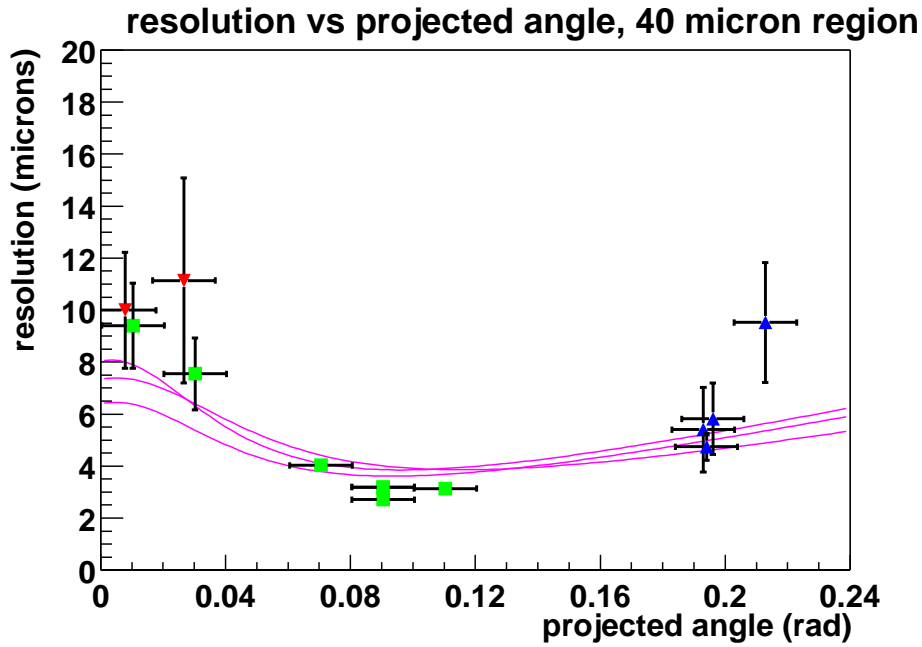
22

Figure 17: The resolution as a function of projected angle for clusters with a fixed number of strips. Red triangles show one-strip clusters, green squares two-strip, and blue triangles three-strip clusters. The fitted resolution for clusters of any size is shown by the pink lines for the three detectors.

From figure 17, it can be concluded that even for a fixed cluster size, the resolution still varies significantly with projected angle. On the other hand, the fitted resolution as a function of projected angle for clusters of all sizes taken together is a good estimate for the resolution. Different resolutions for clusters of different size are not ruled out; if so, however, it is sufficient to describe the resolution as a function of projected angle, which will account for the variations in cluster size.

7.2 Dependence on the Clustering Algorithm

In principle, the above results all depend on the exact definition and cuts of the clustering algorithm. For the operation of the LHCb VELO, it is however highly desirable to obtain a working point where this dependence is small. For the results presented in the previous sections, strips were included in a cluster if the strip signal over noise exceeded 15 ($S/N > 15$).

The analysis was repeated with clusters where this requirement was lowered to $S/N > 5$. In figure 18, the fractions of clusters in this definition containing a given number of strips is shown as a function of projected angle. There is hardly any difference compared to figure 10. The resolution as a function of angle for clusters with a cut $S/N > 5$ is given in figure 19. Again, any differences to the $S/N > 15$ case are marginal. It can be concluded that the resolution, at least for the detectors tested here, is independent of the S/N cut for cut values between 5 and 15. The study needs to be repeated with the final detector technology that is to be used in the LHCb VELO.

8 Measurement of Charge Sharing

The non-zero capacitance between adjacent strips leads to charge sharing, which in turn affects the fraction of clusters that contain a given number of strips for particles traversing the detector at a given projected angle. The charge sharing fraction x is defined such that on a given strip, only a fraction $1-2x$ of the charge is measured, while the two adjacent strips measure a fraction x each if otherwise no charge was deposited there.

The charge sharing fraction has been measured by fitting tracks through five detectors of the telescope, excluding the central r detector in the fit. The tracks are then extrapolated to this detector. Tracks are selected if the projected angle at the point of intercept with the middle r detector is smaller than $50\,\mathrm{mrad}$ and if they pass through the centre of the region between two strips, i.e. if their distance to either strip is more than 40% of the strip pitch. These two strips are called *near* strips in the following. The selection ensures that (even given the effects from charge diffusion, δ rays, and track extrapolation uncertainty) for the two *far* strips that have a distance from the track of ~ 1.5 times the strip pitch, the probability to collect charge deposited by the traversing particle is small. This is confirmed with the study shown in figure 20, where no dependence of the measured charge sharing fraction is observed on the track angle.

Each of these two near strips is considered in turn if the ADC value is greater than 20. For lower ADC values, the information on the charge sharing is diluted by noise. The value of the charge sharing fraction x is then measured from the ADC values on the near strip and the adjacent far strip as follows:

$$x = \frac{\mathrm{ADC_{far}}}{\mathrm{ADC_{near}} + 2\,\mathrm{ADC_{far}}} \ . \tag{20}$$
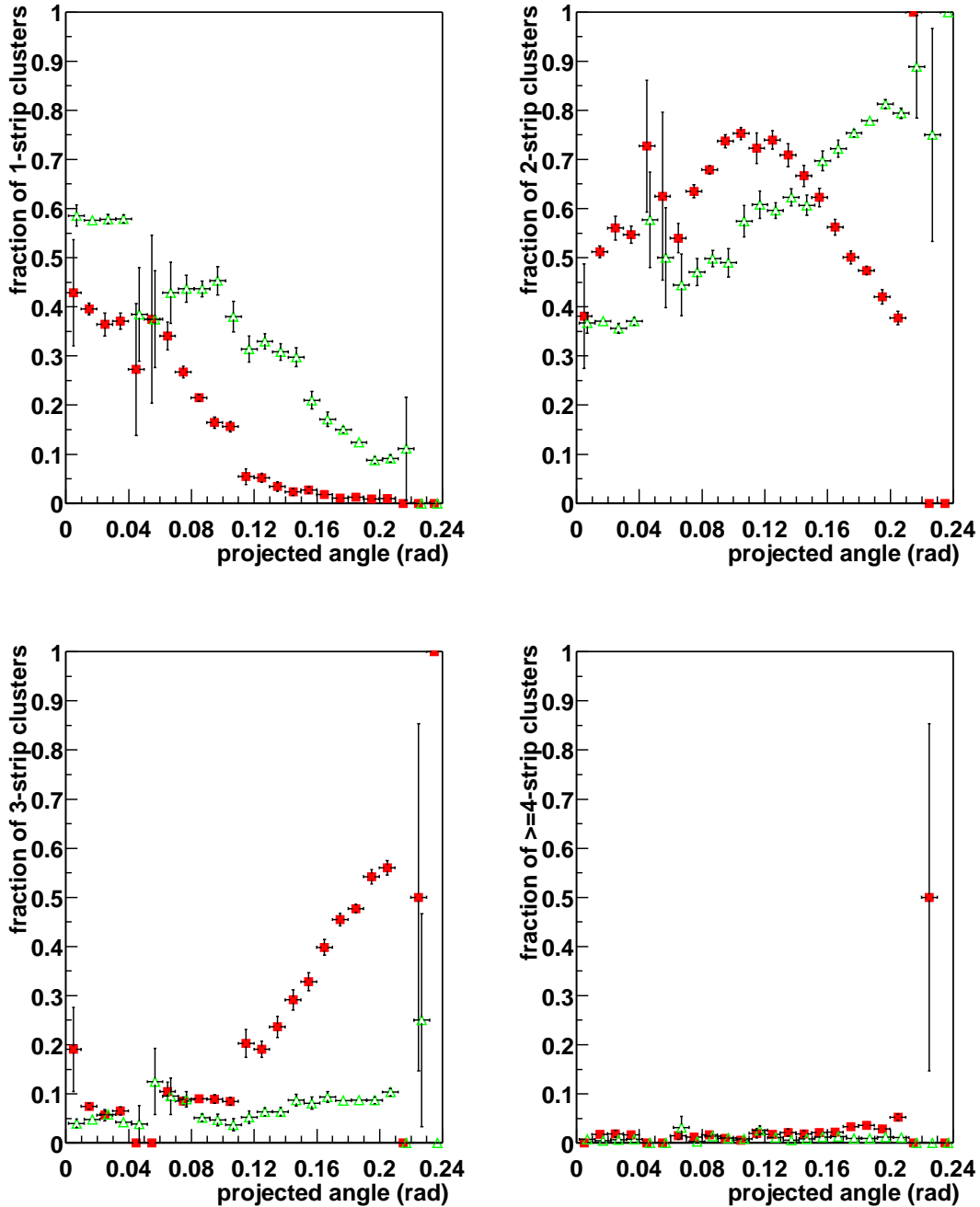
Figure 18: For clusters built with a strip signal to noise cut of $S/N > 5$ instead of 15, the fraction of clusters with a given number of strips as a function of the projected angle of the incident particle is shown. The solid red squares denote the measurement in the $40\,\mu$m pitch region on a $300\,\mu$m thick detector, and the open green triangles correspond to the $60\,\mu$m pitch region. There is no significant difference to the $S/N > 15$ case (cf. figure 10).
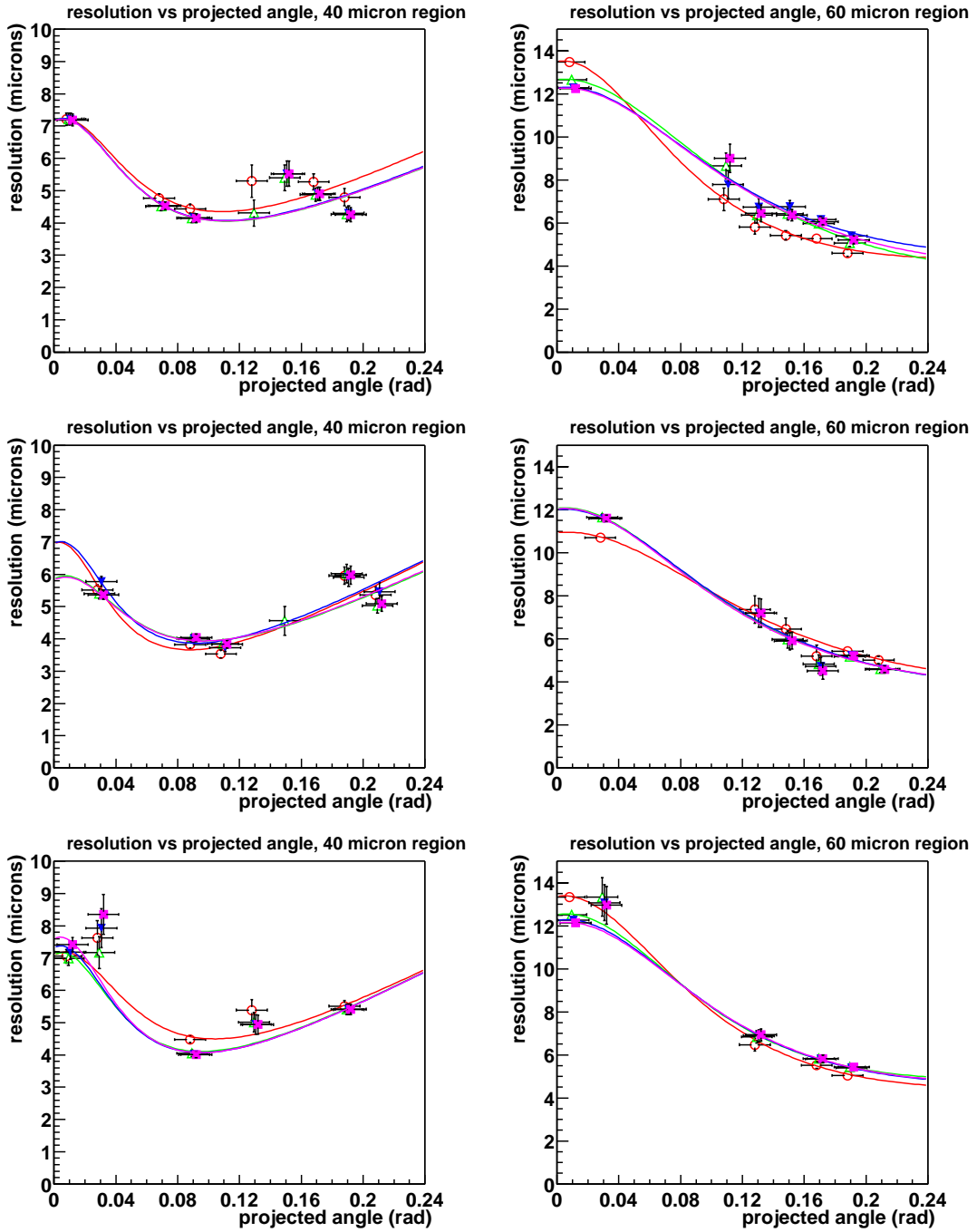
Figure 19: The resolution vs projected angle on the three r detectors, determined from clusters with a $S/N > 5$ cut. The left and right columns show the results for the $40\,\mu$m and $60\,\mu$m pitch regions for the three r detectors, respectively. The points with error bars denote the measured resolution, with red circles, green triangles, blue triangles, and pink squares corresponding to the first to fourth iterations, respectively. The points have been slightly offset horizontally for better visibility. The fitted resolution as a function of projected angle is shown for each iteration in the corresponding colour. There is no significant difference to the $S/N > 15$ case (cf. figure 14).
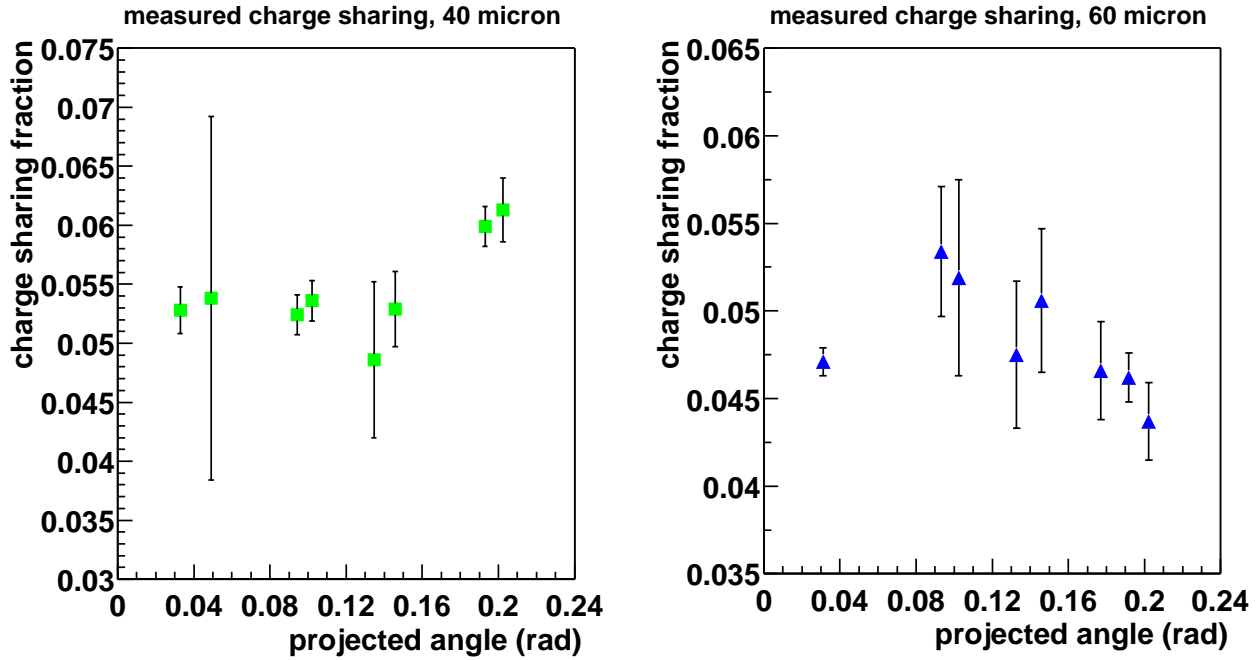
Figure 20: The measured charge sharing fraction as a function of projected angle of the tracks. All points are statistically independent. There is no dependence on the track angle except for very large angle tracks passing through the $40\,\mu$m pitch region corresponding to a distance perpendicular to the strips l_p of about $60\,\mu$m, which is the angle at which the far strip starts to collect deposited charge.

The measured values of x are shown in figure 21, separately for $40\,\mu$m and $60\,\mu$m pitch. A Gaussian fit to the center of the distribution yields

$$
\begin{aligned}
x(40\,\mu\mathrm{m}) &= (5.3 \pm 0.3 \pm 0.1(\mathrm{syst.}))\% \quad \text{and} \\
x(60\,\mu\mathrm{m}) &= (4.7 \pm 0.1 \pm 0.2(\mathrm{syst.}))\%\,.
\end{aligned}
\tag{21}
$$

These values do not depend significantly on the extent of the central area between the strips or the cuts on the projected angle and the ADC value of the near strips. When performing the fit separately for strips at larger/smaller radii than the extrapolated track position, the results differ by 0.1% (0.2%) from the quoted value for the $40\,\mu$m ($60\,\mu$m) region. These differences could be due to residual misalignment and are assigned as systematic errors.

9   Simulation

The resolution measurement presented in section 7 is compared both to the current version of SICb and with a more sophisticated simulation, which will replace the crude model in SICb in the future.

9.1   Comparison to the Model in SICb v234

In the SICb v234 model, uniform non-zero noise is assumed on the silicon detectors. In the charge collection process, lateral diffusion is not taken into account, inter-strip capacitive coupling is neglected, and δ rays are not simulated. For comparison with the measurements
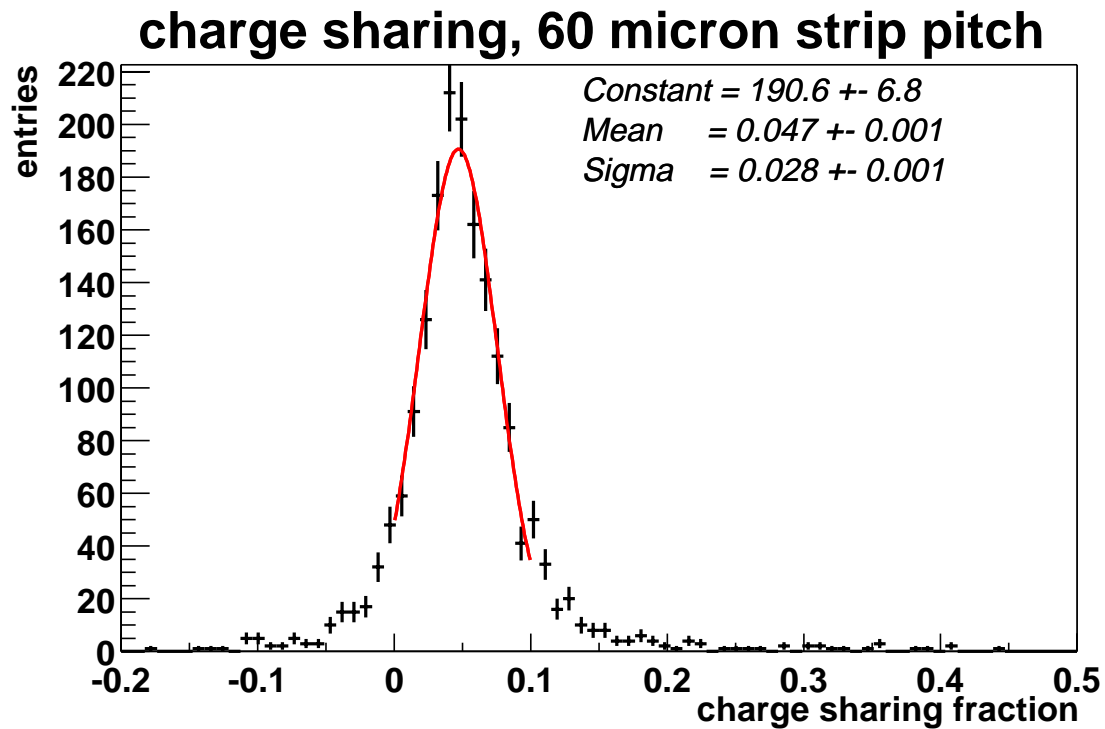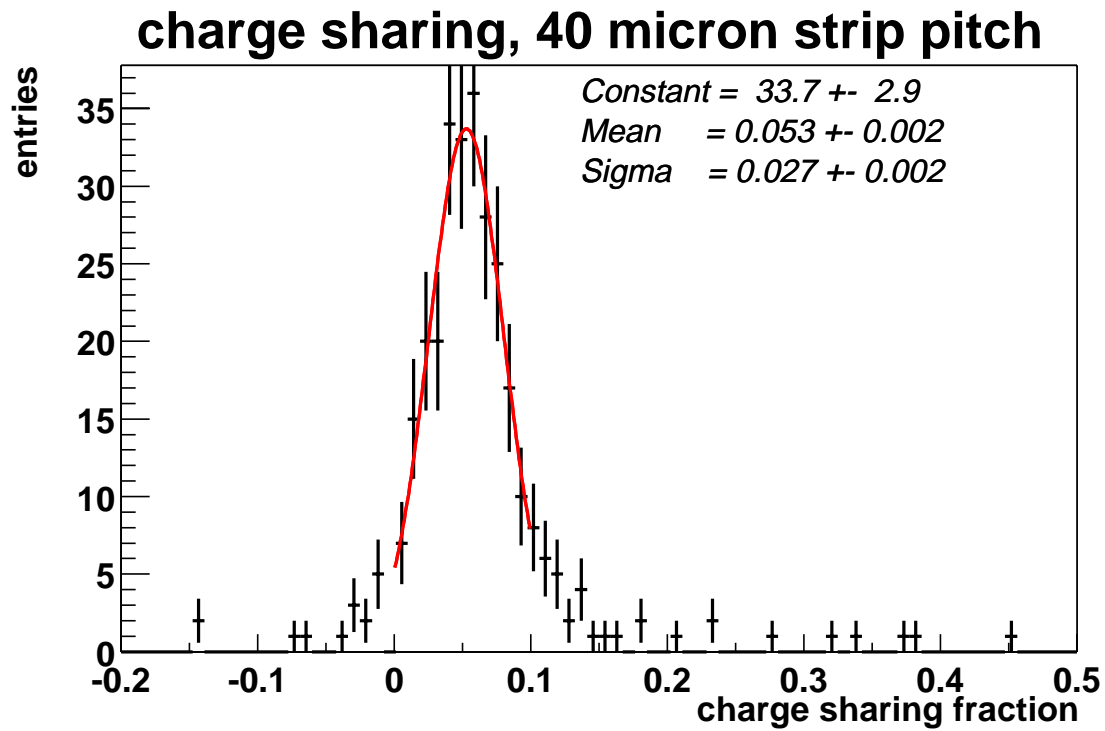
Figure 21: The measured charge sharing fractions x for different strip pitch. The red curves indicate Gaussian fits to the distributions; the fitted parameters are given in the plots. The width of the distributions is consistent with the expectation from noise fluctuations.

presented in this note, SICb has been used to simulate detectors of $300\,\mu$m thickness. The resolution as a function of projected angle is shown in figure 22 for SICb v234. It can be seen that the best resolution is roughly reproduced at the correct track angle, while the resolution for perpendicular tracks is not good enough since no diffusion is included.

9.2   Improved Simulation

Currently, a simulation of the charge collection process in silicon detectors based on [5] is being developed for future use in the LHCb Monte Carlo simulation. The main additional features of this simulation are

1. inhomogeneous charge distribution along the track,
2. diffusion during charge collection,
3. emission of δ-rays above an energy cutoff $T_{\text{cut}} = 70\,$keV, and
4. capacitive charge coupling between strips.

Clusters are formed according to the procedure described in section 3. Throughout this section the weighted cluster position (weighting each strip by its signal) is taken as the reconstructed cluster position unless stated otherwise.

Charge distribution   The deposition of charge along the track is done using the GEANT [6] Urban model (following roughly a Vavilov distribution) in $5\,\mu$m-long segments with an energy cutoff of T_{cut}. It has been checked that the use of shorter segments does not affect the resolution (but increases the CPU time).

The shape of the total cluster charge is shown in figure 23. The width of the simulated Landau distribution is slightly narrower in the simulation than in the data. However, the results concerning the resolution are not sensitive to the exact modelling of the ratio of the width and the most probable value of the Landau, since the S/N cut in the cluster making is below the lower edge of the Landau. Figure 24 shows the resolution one would get without diffusion, δ-rays and charge sharing, which are discussed below. This crude simulation is comparable to what is done in SICb except a homogeneous charge distribution is assumed there.

Diffusion   The lateral diffusion of charge carriers depends on the temperature, the voltage and the diffusion distance. At $V = 80\,$V, $kT = 0.025\,$eV and a thickness of $300\,\mu$m the rms of the distribution is $6\,\mu$m, which defines a lower limit for the precision of any other effects to be considered in the simulation. Because of diffusion the average cluster size increases, which has a positive effect on the resolution of perpendicular tracks as one can see from figure 24.

Knock-on electrons (δ-rays)   The distribution of δ-rays of kinetic energy T ($T < T_{\text{max}}$, the maximal energy that can be imparted to a free electron) follows [7]

$$\frac{d^2N}{dT\,dx} \propto \frac{1 - \beta^2 \frac{T}{T_{\text{max}}}}{\beta^2 T^2}, \tag{22}$$

where β denotes the velocity of the particle traversing the silicon detector, normalised to the speed of light. In this simulation only δ-rays above an energy cut of $T_{\text{cut}} = 70$ keV were considered. This corresponds to a mean path in silicon of the order of the scale defined by lateral diffusion. The recoil angle of δ-rays is peaked close to $\pi/2$, and some δ electrons may traverse up to a few hundred microns of silicon, which significantly degrades the resolution especially at large track angles (see figure 24).
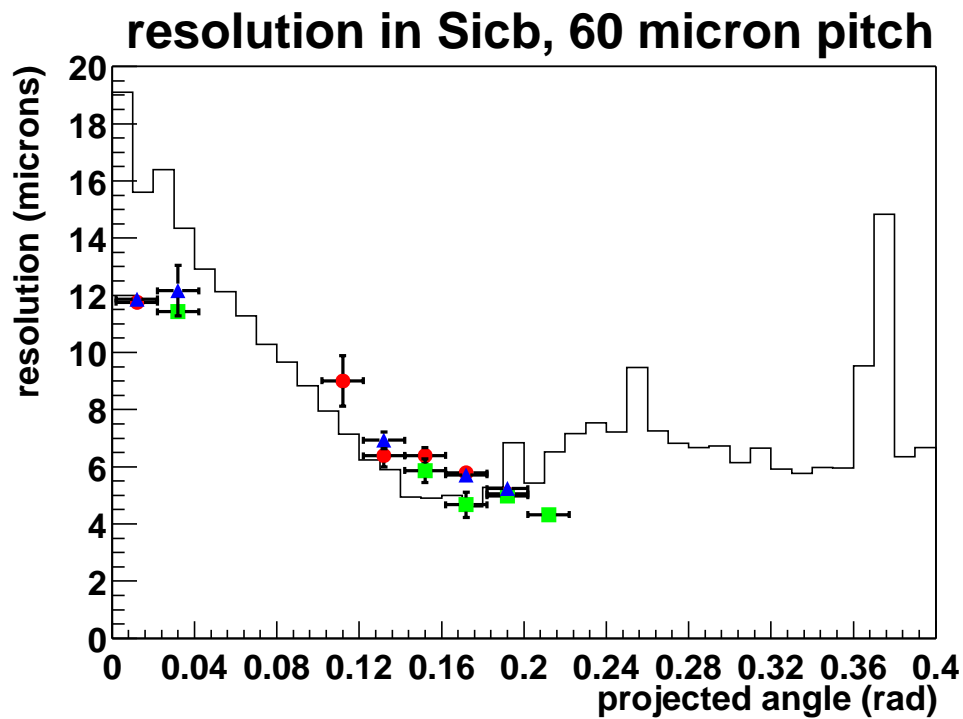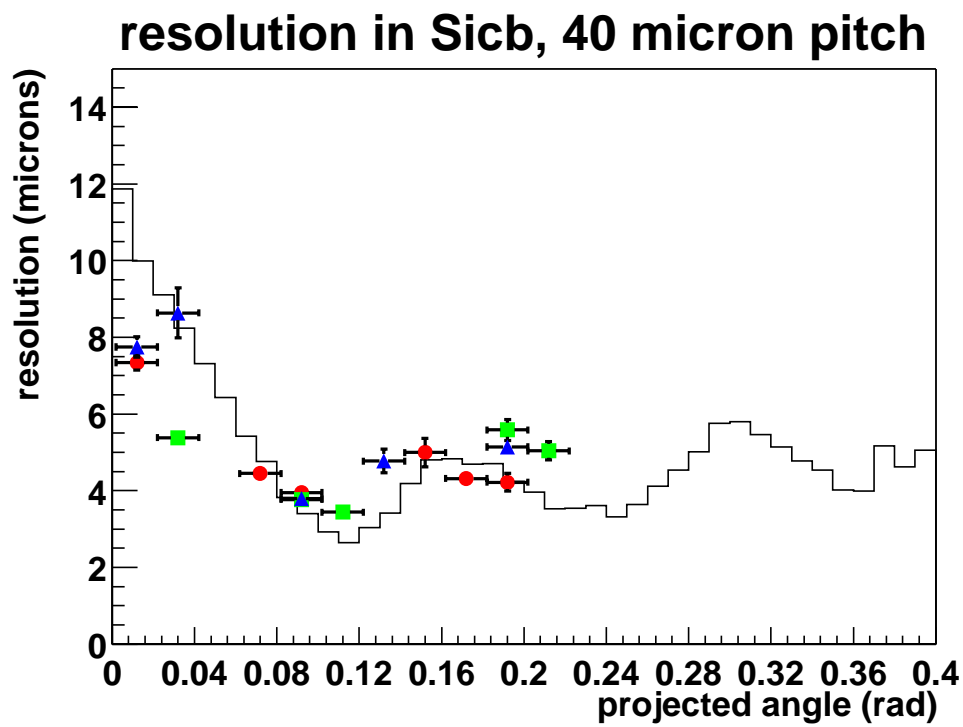
Figure 22: The resolution for detectors of $300\,\mu$m thickness as a function of track angle as simulated in SICb v234 is shown by the solid histograms for $40\,\mu$m and $60\,\mu$m pitch. The measured resolution as shown in figure 15 is overlaid.
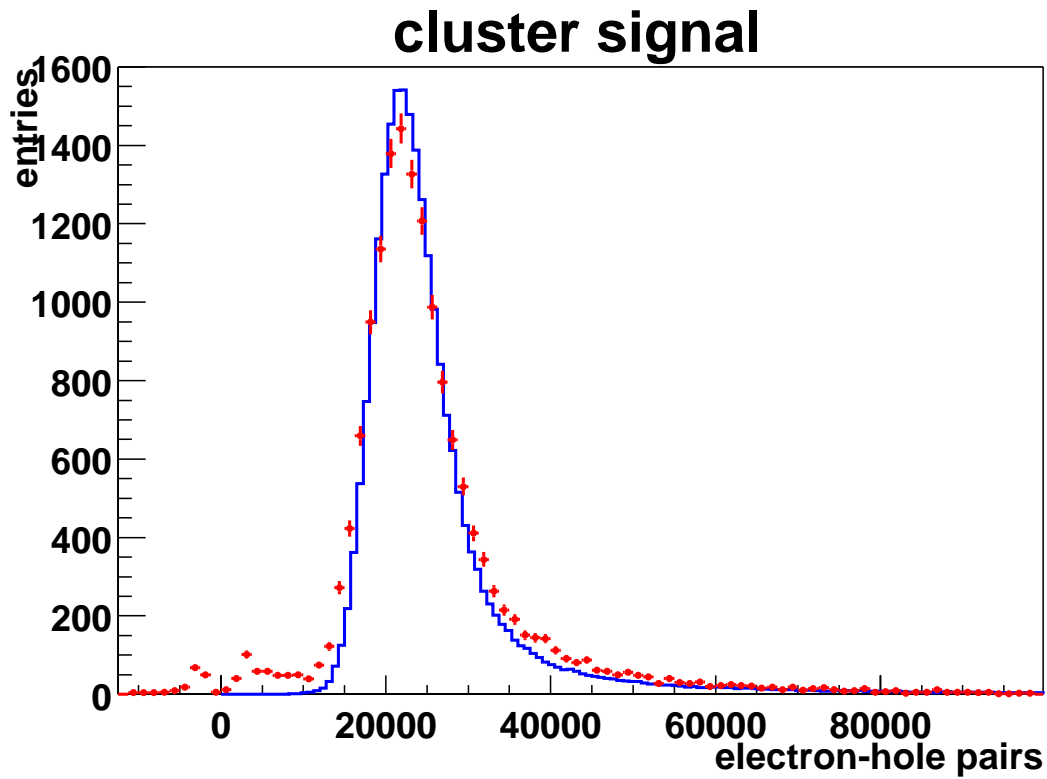
Figure 23: Compared measured and simulated Landau distributions. The conversion factor from measured cluster ADC values to the number of electron-hole pairs has been set to 250 so that the most probable values coincide.
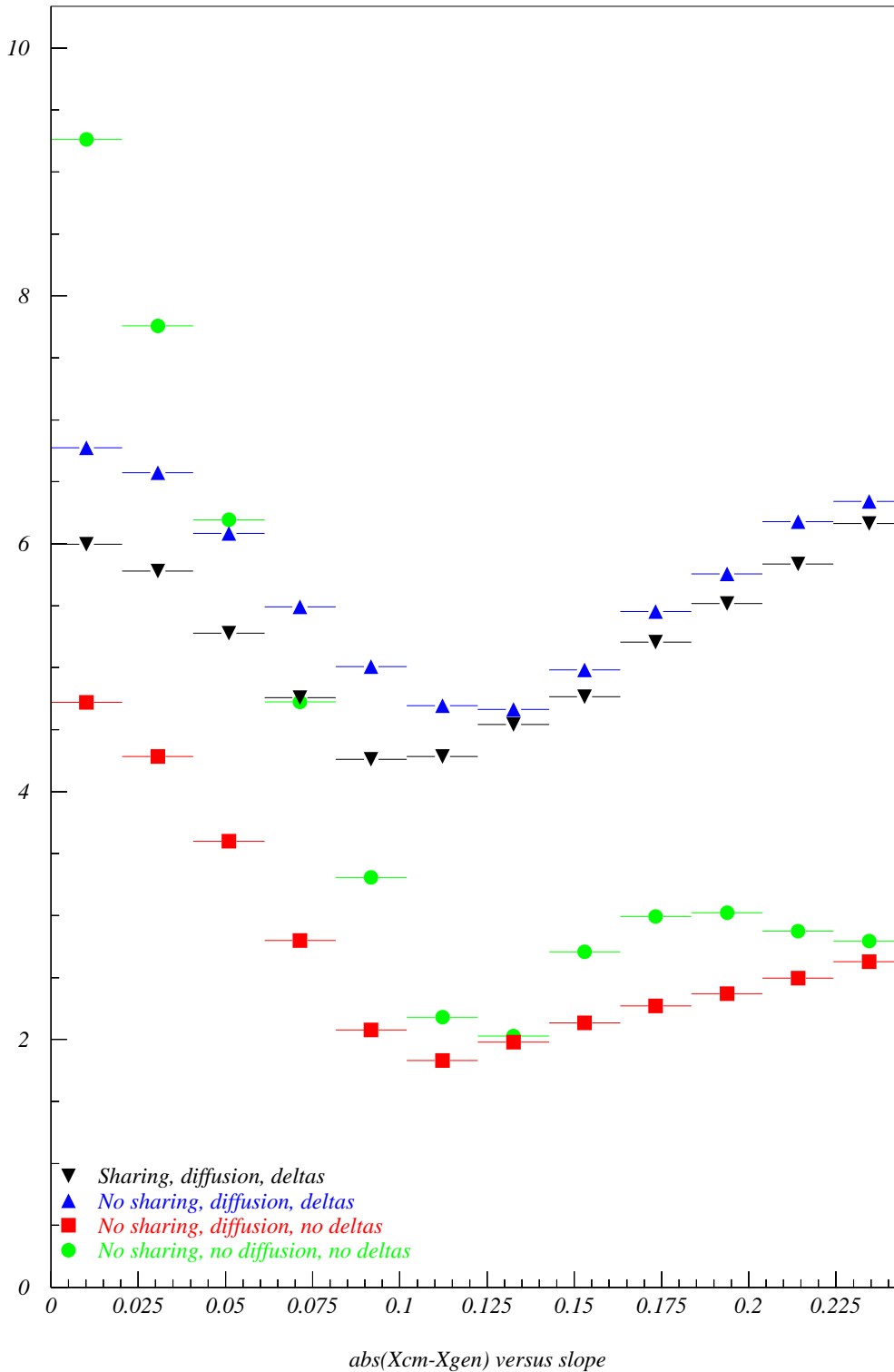
Figure 24: Simulated resolution (in μm) as a function of projected angle (in rad) together with the effects of diffusion, δ-rays and charge sharing. The values correspond to a $300\,\mu$m thick detector with $40\,\mu$m strip pitch. A flat distribution of track angles was generated in the simulation; if only perpendicular tracks were contained in the first bin, the resolution for purely geometric charge collection (no charge sharing, diffusion, or δ ray emission) would otherwise be $40\,\mu\text{m}/\sqrt{12} = 11.5\,\mu$m.

Capacitive coupling (charge sharing) The non-zero capacitance between adjacent strips leads to charge sharing, as measured in section 8. Charge sharing in turn affects the fraction of clusters that contain a given number of strips at a given track angle. We consider that a given strip measures a fraction of $(1 - 2x)$ of the charge it collects and its neighbours a fraction x each. In the simulation, the value of the charge sharing parameter has been set to $x = 5\%$, see section 8.

The effect of the charge sharing fraction on the fraction of 1-strip clusters for perpendicular tracks has been studied in more detail and is summarised in table 1. A charge sharing fraction of 5% reproduces well the fractions of clusters with different numbers of strips for all track angles, see figure 25.

x	0%	2%	4%	5%	6%	7%	8%	10%	
40μm pitch	53%	49%	42%	40%	34%	25%	20%	3%	$\pm 2\%$
60μm pitch	67%	64%	61%	59%	51%	41%	27%	4%	$\pm 2\%$

Table 1: Fractions of 1-strip clusters for perpendicular tracks depending on the charge sharing fraction x.

With these parameters, the simulated resolution versus angle shown in figure 26 agrees within errors with the measurements for $40\,\mu$m and $60\,\mu$m strip pitch. The simulation can then be used in order to evaluate different VELO detector layouts before the actual beam test. A qualitative discussion is given in section 9.4.

9.3 Improved resolution using an η-fit

Figure 24 shows that charge sharing *improves* the resolution for low angle tracks. This is a consequence of the way the cluster position x_{cm} is calculated using the charge weighted centre approximation.

In figure 27, the left top plot shows the reconstructed $x_{\text{cm}} - x_{\text{true}}$ position for tracks with an angle below 20 mrad. To understand the two-peaked shape mainly due to 2-strip clusters, one introduces:

$$\eta = \frac{S_1}{S_1 + S_2} \tag{23}$$

where S_i is the signal in strip i. Clearly

$$x_{\text{cm}} = \eta \cdot \text{pitch}. \tag{24}$$

The x_{true} versus η curve is shown in the bottom plot. The definition of x_{cm} is equivalent to considering this curve as a straight line. A fit of this curve leads to a set of functions

$$x_\eta = F_{\alpha_p}(\eta) \tag{25}$$

at fixed projected angle. The curve is well described by a function of the form

$$x_\eta = \frac{p}{2} + a_{\alpha_p}(\eta - 0.5) + b_{\alpha_p}(\eta - 0.5)^3 \tag{26}$$

where p denotes the strip pitch and the parameters a_{α_p} and b_{α_p} are determined in a fit to the curve for a given range of projected angles α_p. The residual distribution $x_\eta - x_{\text{true}}$ is shown in
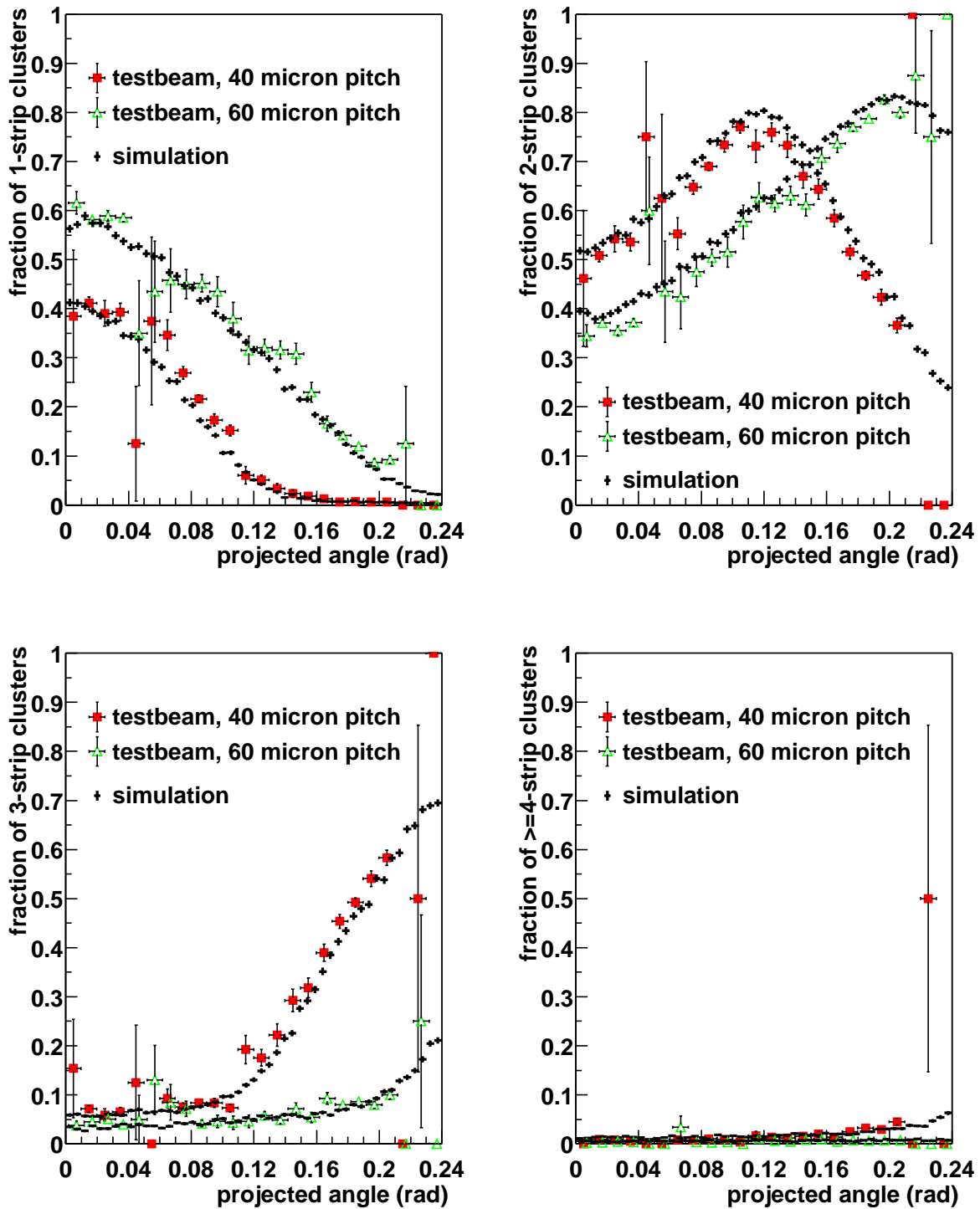
33

Figure 25: The simulated fractions of 1, 2, 3 and n-strip ($n > 3$) clusters versus projected angle for $40\,\mu$m and $60\,\mu$m strip pitches as indicated by the small points are compared to the testbeam measurements.
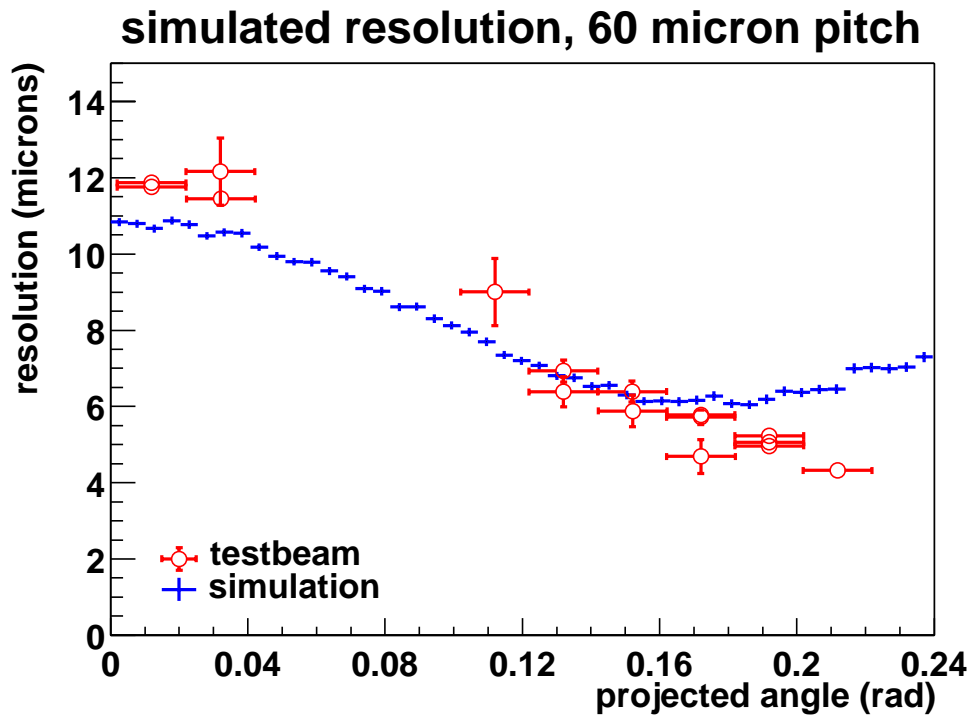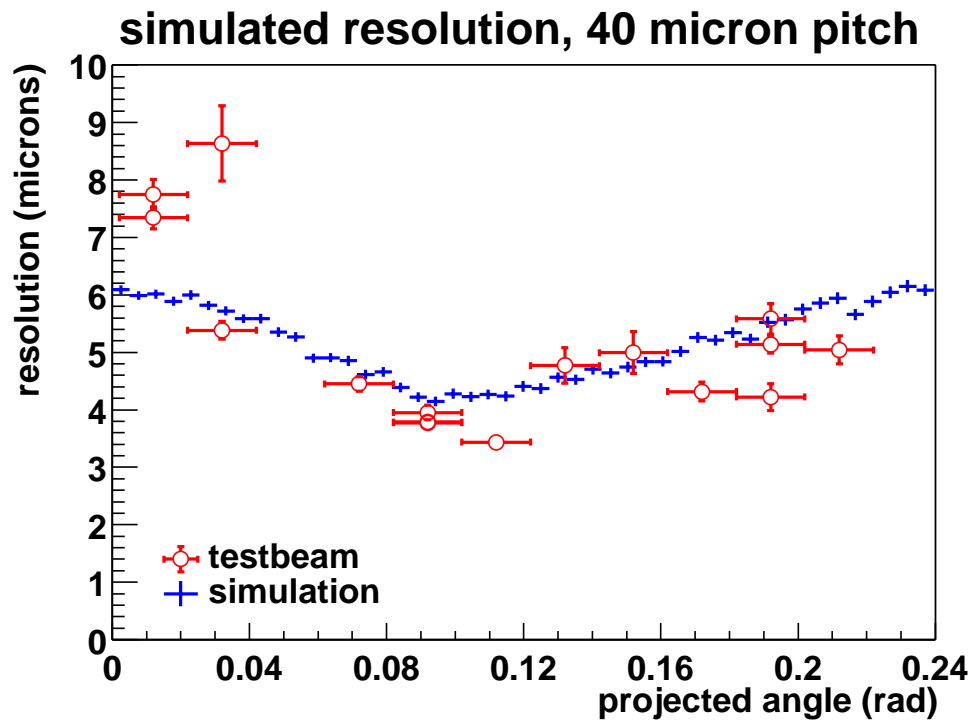
Figure 26: Simulated and measured resolution as a function of projected angle for $300\,\mu$m thick detectors.
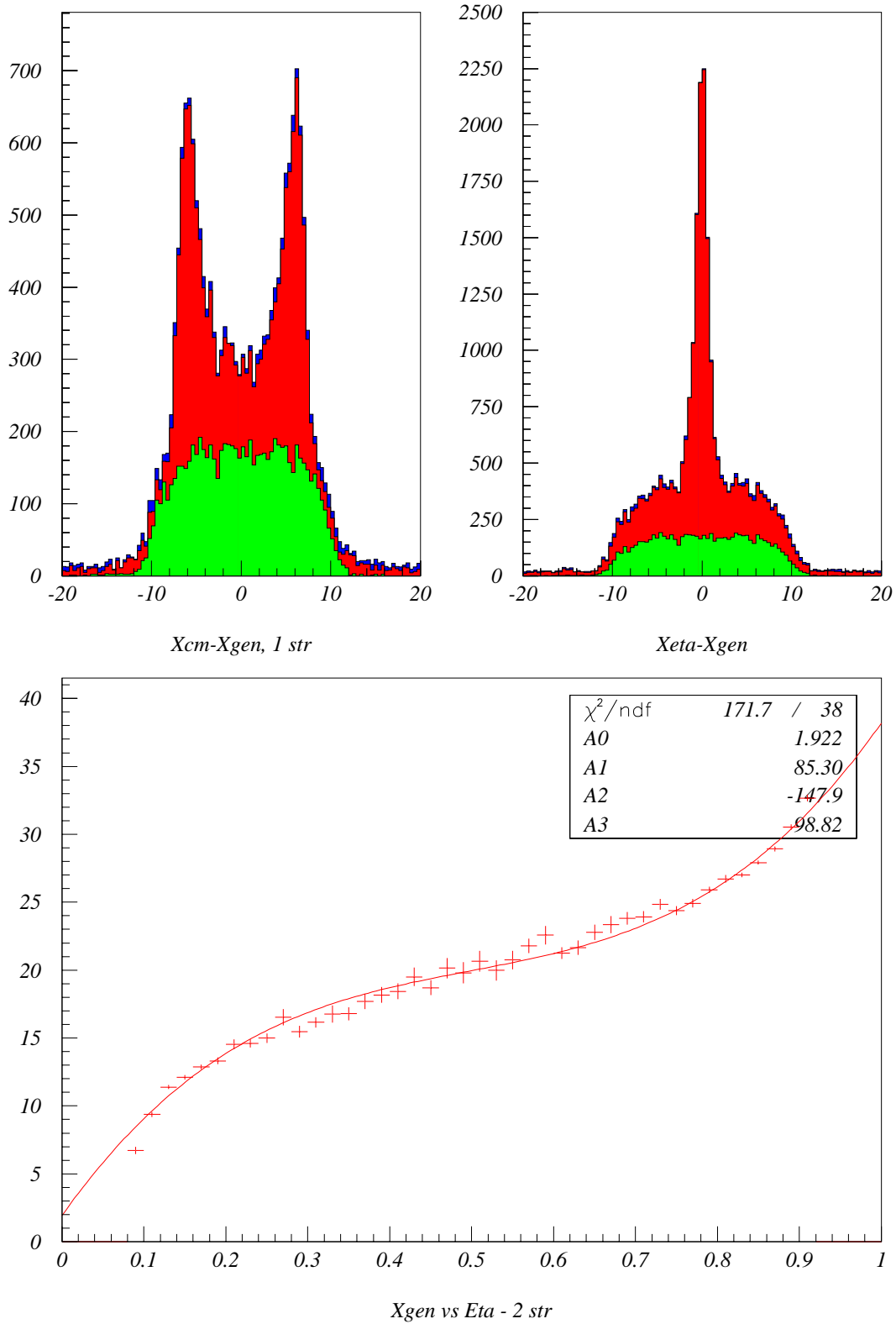
Eta fit for perpendicular tracks

χ²/ndf	171.7 / 38
A0	1.922
A1	85.30
A2	-147.9
A3	98.82

Figure 27: Top: $x_{\mathrm{cm}} - x_{\mathrm{true}}$ (left) and $x_\eta - x_{\mathrm{true}}$ for perpendicular tracks in $40\,\mu\mathrm{m}$ micron strips. The contributions of 2-strip clusters are shown in red (green: 1-strip clusters, blue: n-strip clusters ($n > 2$)). Bottom: x_{true} in $\mu\mathrm{m}$ versus η for 2-strip clusters at $40\,\mu\mathrm{m}$ pitch. The fitted parameters p_1 and p_2 correspond to the parameters a and b in equation 26, respectively.

the top right plot, where the contributions of 1- and n-strip ($n > 2$) clusters remain unchanged. Note that practically x_η can only be calculated in a second iteration once the pattern recognition algorithm found the projected angle of incidence of the track.

The anticipated effect on the overall resolution is shown in figure 28. A large improvement in the resolution seems to be possible, especially for tracks at low angles. For clusters containing three or more strips, the expected improvement from the same algorithm has been found to be marginal, and thus no large change is expected in the resolution for clusters at large projected angles. A comparison with data will be done in a future study.

9.4   Tracks in the LHCb VELO

For the VELO operation in LHCb, two factors enter the track impact parameter resolution: the geometrical extrapolation precision back to the interaction region, determined from the position of the hits on the track, and the resolution of these hits themselves. Both depend on the angle of the track with respect to the beam axis, and for the VELO optimisation, it would be desirable if the angle at which the best single hit resolution is obtained matched the angles that give the best geometrical extrapolation resolution.

Tracks close to the beam only hit the very forward detectors and therefore have a long extrapolation to the primary interaction point, while tracks at very large angles leave the VELO acceptance after traversing few stations and have only a short lever arm. In figure 29 the geometrical resolution in units of the single hit resolution is shown versus track angle for the VELO design of the technical proposal [8]. The best geometrical resolution is obtained for tracks at ≥ 40 mrad.

Figure 30 on the other hand shows the predicted single hit resolution for the $220\,\mu$m thick detectors of the VELO baseline design layout presented in [9] and for various strip pitches. Note that for strip pitches below $20\,\mu$m the best resolution is obtained for perpendicular tracks (rather than for tracks at a non-zero projected angle) because for small pitch and large angles, the average number of strips per cluster increases to a level that the signal over noise ratio may fall below the cut in a significant fraction of cases. For angles of more than ~ 150 mrad a strip pitch below $20\,\mu$m actually leads to a deterioration of the resolution. The case of $300\,\mu$m thick detectors corresponding to the VELO backup layout discussed in [9] leads to similar conclusions; here, the preferred strip pitch is $25\,\mu$m.

For a strip pitch above $30 - 35\,\mu$m, the angle $\alpha_{\text{single hit}}$ at which the best single hit resolution is expected roughly scales as

$$\alpha_{\text{single hit}} \sim (80 - 120\,\text{mrad}) \cdot \frac{300\,\mu\text{m}}{\text{thickness}} \cdot \frac{\text{pitch}}{40\,\mu\text{m}} \ . \tag{27}$$

To match the angular range of ≥ 40 mrad in which the best extrapolation precision is achieved using detectors that have a strip pitch of around $40\,\mu$m, these detectors would have be even thicker than 300μm. Thus, for the detectors of the VELO baseline design a strip pitch in the inner regions of the r detectors of around $20\,\mu$m would yield the optimal impact parameter resolution over the whole range of relevant angles in LHCb. The optimum pitch is $\sim 25\,\mu$m for the backup solution. The question of the cluster finding efficiency still has to be addressed. For the ϕ detectors, where the projected angle is limited to the stereo angle of the strips, the finest possible strip pitch at the inner radius is preferable.
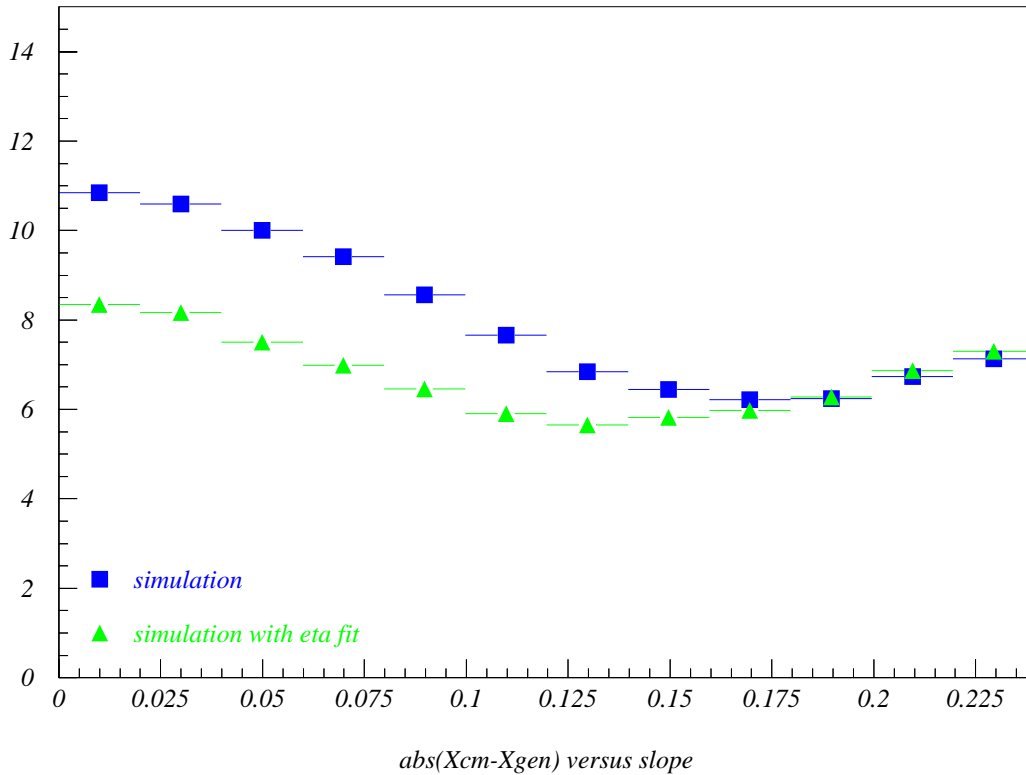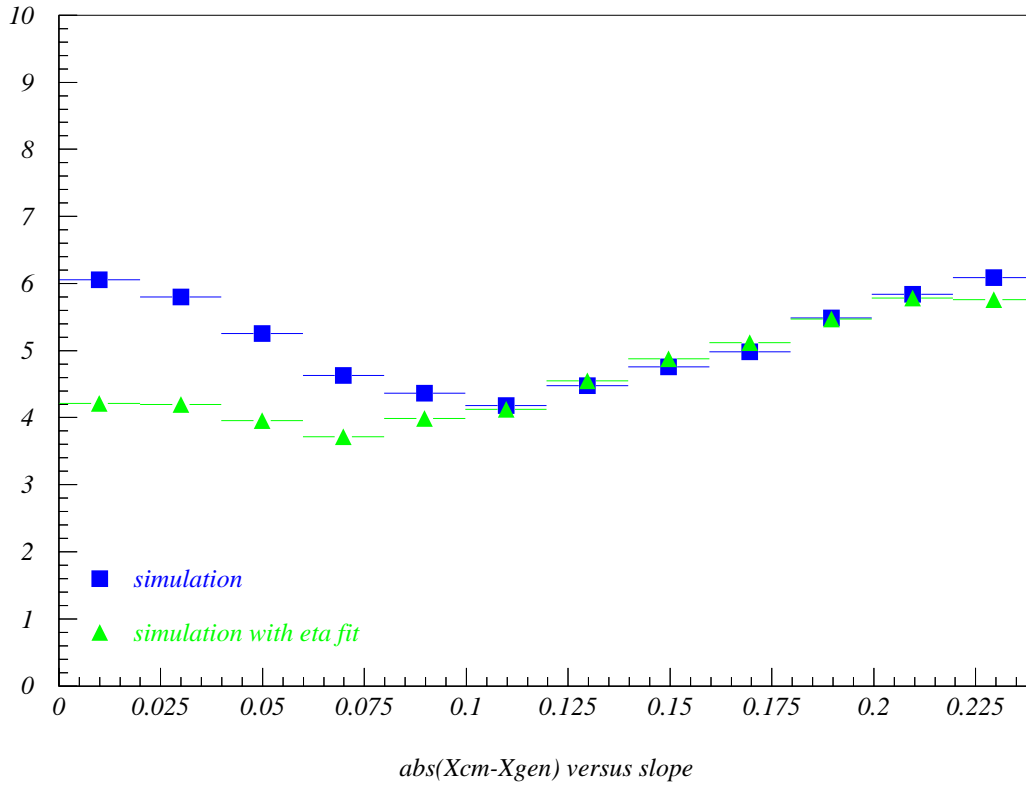
Figure 28: The resolution (in μm) as expected from the simulation as a function of projected angle (in rad). The upper plot corresponds to 40 μm, the lower to 60 μm strip pitch on a 300 μm thick detector. Results are shown for x_{cm} (blue squares) and for x_{η} (green triangles).
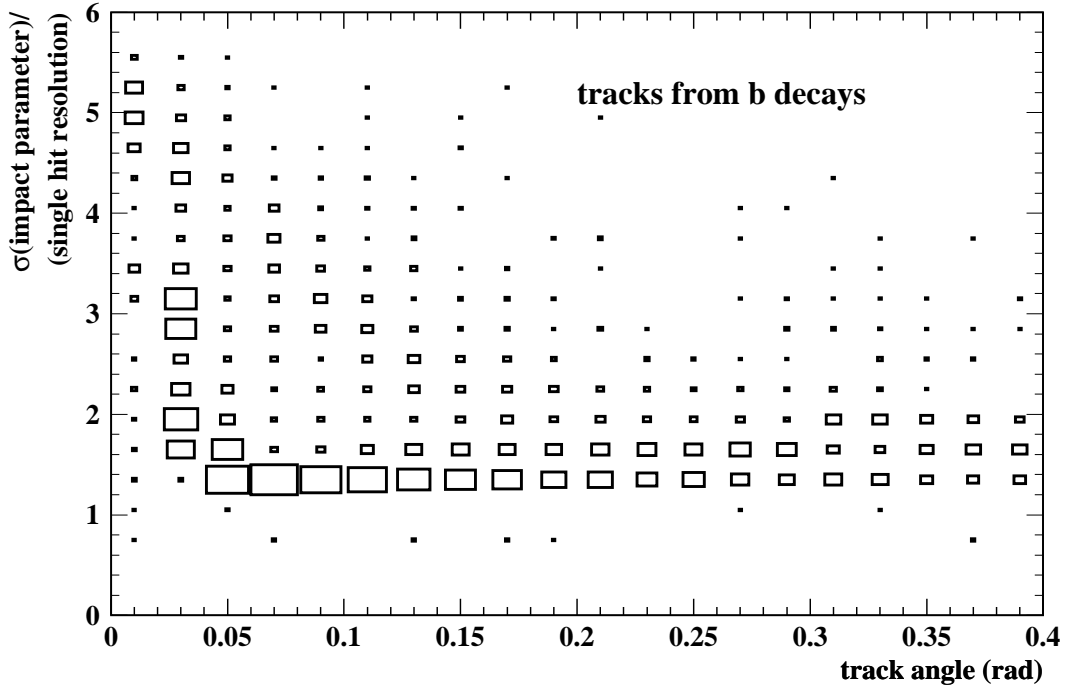
Figure 29: The extrapolation precision of tracks in the VELO to the primary interaction point in units of the single hit resolution vs. the angle of the tracks. Shown are all b decay products in events containing a $B^0 \to \pi^+\pi^-$ decay. The VELO setup is that of the technical proposal.

10   Conclusion

In this note, results of a beam test of the $300\,\mu$m thick n-on-n 1998 VELO prototype detectors have been presented. The efficiency has been analysed as a function of bias voltage, and the inefficiencies due to effects of the silicon detectors determined separately from those due to noisy or dead channels on the readout chips. It has been found that a safe operating point is at $90\,$V bias voltage or above (cf. figure 9) where the efficiency is very close to $100\,\%$ and the main part of the $\mathcal{O}(1\,\%)$ loss of efficiency is due to noisy or dead channels. Below $90\,$V and above $70\,$V, neither r nor ϕ detectors show a decrease of the efficiency when noisy or dead channels have been accounted for. However, the number of noisy channels on the r detectors does increase below $90\,$V. Below $70\,$V the efficiency drops drastically on all detectors. A large local variation of the inefficiencies is observed.

The resolution of the detectors has been studied as a function of incident angle of the measured particle. A large variation of the resolution has been observed, see figure 15. For perpendicular tracks, the resolution in the $40\,\mu$m and $60\,\mu$m regions is $7-8\,\mu$m and $\sim 12\,\mu$m, respectively. The following best resolutions have been obtained:

strip pitch	projected angle	resolution
$40\,\mu$m	$80-120\,$mrad	$3.6-3.9\,\mu$m
$60\,\mu$m	$\geq 200\,$mrad	$4.0-4.6\,\mu$m

With the simple clustering algorithm used (assigning a weight proportional to the signal in each strip to determine the cluster position), the main dependence of the resolution is on the track angle, rather than the number of strips in a cluster at a given angle.
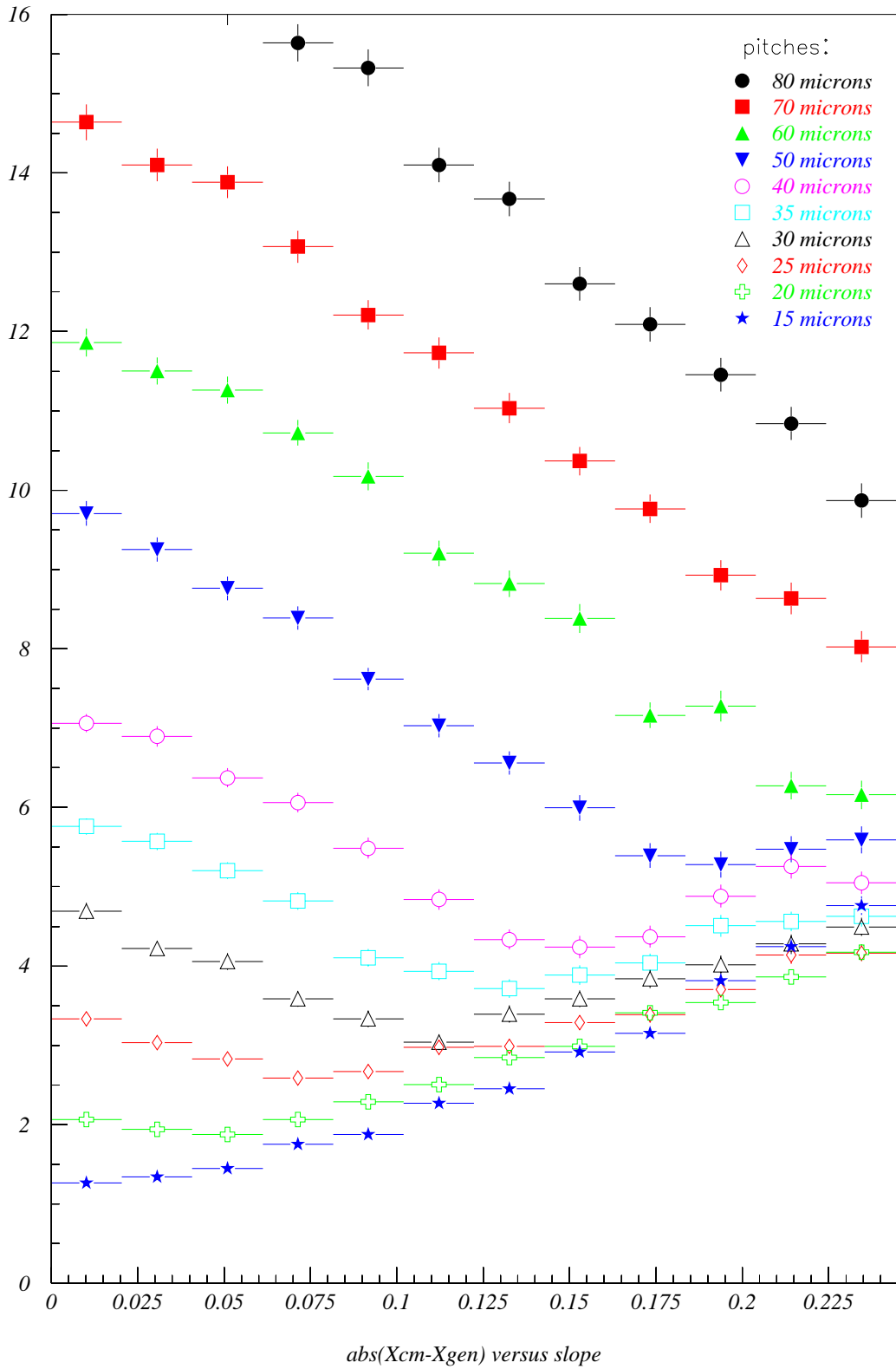
Figure 30: Simulated center-of-mass resolution in μm versus projected angle in rad at various strip pitches for a $220\,\mu$m thick detector.

Inter-strip capacitive coupling leads to charge sharing between adjacent strips, such that only a fraction $(1-2x)$ of the charge is measured on the strip itself while a fraction x is measured on each of the two neighbours. For the 1998 VELO prototypes, the charge sharing fraction has been measured to be $(5.3 \pm 0.3 \pm 0.1)\%$ in the $40\,\mu$m pitch region and $(4.7 \pm 0.1 \pm 0.2)\%$ for $60\,\mu$m pitch.

The results of the resolution study have been compared with a detailed simulation of the silicon detectors. The fraction of clusters with a given number of strips as a function of angle and the resolution as a function of angle have been investigated. The interstrip capacitance is simulated with a simple interstrip charge sharing fraction of $5\,\%$, and the data are well reproduced by the simulation. The results have been found to be insensitive to the exact parameterisation of the Landau describing the particles' energy loss in the detector, since the signal over noise cut in the clustering algorithm is above the lower edge of the spectrum.

The simulation suggests that the true position is not a linear function of the signal fraction η in one of the strips of a 2-strip cluster. When taking this dependence into account, a significant improvement in the resolution should be possible, especially for almost perpendicular tracks. This will be studied in a future LHCb note.

A qualitative study of the optimal strip pitch for the VELO detectors has been presented. Based on the new VELO simulation, this analysis will be continued in the future in more detail, taking into account predictions for the cluster finding efficiency.

The current version of the VELO simulation in SICb takes noise into account, but neither diffusion nor inter-strip capacitive coupling. (Also, neither noisy nor dead strips are accounted for.) Nevertheless, the overall picture of the resolution as a function of angle agrees with the measurements shown here, although the best resolution occurs at an angle that is roughly twice as large since $150\,\mu$m thick detectors are assumed in SICb.

References

[1] S. Saladino, *Study of vertex silicon detectors for LHC experiments*, thesis (CERN-OPEN-99-374), 3 December 1999.

[2] O. Toker, S. Masciocchi, E. Nygard, A. Rudge and P. Weilhammer, Nucl. Instrum. Meth. **A340** (1994) 572.

[3] I. Tomalin, *Alignment of the 1998 VELO test beam*, LHCb VELO 99-032, internal note, 27. 8. 1999.

[4] R. J. Barlow, *Statistics: a guide to the use of statistical methods in the physical sciences*, Manchester physics series, Wiley 1989.

[5] P. Koppenburg, *Comparison of analogue and binary read-out in the silicon strips vertex detector of LHCb*, LHCb TRAC 97-020

[6] *Geant - Detector description and Simulation Tool*, CERN Program Library Long Writeup W5013

[7] D. E. Groom *et al.*, *The Review of Particle Physics*, The European Physical Journal C15, 1 (2000)

[8] The LHCb Collaboration, *Technical Proposal for A Large Hadron Collider Beauty Experiment for Precision Measurements of CP Violation and Rare Decays*, CERN/LHCC 98-4, LHCC/P4 (20. 2. 1998).

[9] T. Bowcock *et al.*, *VELO Geometry Optimisation*, LHCb VELO 2000-25.

A Residual Widths and Extrapolation Precision: A Special Case

For the special case of three detectors with equal resolution σ placed at z positions $-z_0$, 0, and $+z_0$, the widths of the residual distributions can be derived from the formulae in section 6.2 as follows:

From equations 11 and 12,

$$\frac{\partial \overline{y}}{\partial y_k} = \frac{1}{\sigma^2 \sum\limits_{i=1}^{n} \frac{1}{\sigma^2}} = \frac{1}{3} \quad \text{and} \tag{28}$$

$$\frac{\partial (\overline{yz})}{\partial y_k} = \frac{z_k}{\sigma^2 \sum\limits_{i=1}^{n} \frac{1}{\sigma^2}} = \frac{z_k}{3} \ . \tag{29}$$

Then, equations 9 and 10 yield

$$\frac{\partial m}{\partial y_i} = \frac{1}{\frac{2}{3} z_0^2} \left(\frac{z_i}{3} - 0 \right) = \frac{z_i}{2 z_0^2} \quad \text{and} \tag{30}$$

$$\frac{\partial c}{\partial y_i} = \frac{1}{3} - \frac{\partial m}{\partial y_i} \cdot 0 = \frac{1}{3} \ . \tag{31}$$

From equations 8 and 7, one has for an outer detector:

$$\frac{\partial \Delta y_1}{\partial y_1} = 1 - \left(\frac{-z_0}{2 z_0^2}(-z_0) + \frac{1}{3} \right) = \frac{1}{6}$$

$$\frac{\partial \Delta y_1}{\partial y_2} = -\left(0 + \frac{1}{3} \right) = -\frac{1}{3}$$

$$\frac{\partial \Delta y_1}{\partial y_3} = -\left(\frac{z_0}{2 z_0^2}(-z_0) + \frac{1}{3} \right) = \frac{1}{6}$$

$$\Rightarrow \sigma_{\Delta y_1} = \sigma \sqrt{\left(\frac{1}{6} \right)^2 + \left(\frac{1}{3} \right)^2 + \left(\frac{1}{6} \right)^2} = \sqrt{\frac{1}{6}} \sigma \ . \tag{32}$$

Similarly, for the middle detector:

$$\frac{\partial \Delta y_2}{\partial y_1} = -\left(0 + \frac{1}{3} \right) = -\frac{1}{3}$$

$$\frac{\partial \Delta y_2}{\partial y_2} = 1 - \left(0 + \frac{1}{3} \right) = \frac{2}{3}$$

$$\frac{\partial \Delta y_2}{\partial y_3} = -\left(0 + \frac{1}{3} \right) = -\frac{1}{3}$$

$$\Rightarrow \sigma_{\Delta y_2} = \sigma \sqrt{\left(\frac{1}{3} \right)^2 + \left(\frac{2}{3} \right)^2 + \left(\frac{1}{3} \right)^2} = \sqrt{\frac{2}{3}} \sigma \ . \tag{33}$$

The extrapolation precision for the same case can be computed as follows. Equation 16 yields

$$
\frac{\partial y}{\partial y_1} = \frac{1}{3}\left(\frac{z(-z_0)}{\frac{2}{3}z_0^2} + 1\right) = \frac{1}{3}\left(-\frac{3}{2}\frac{z}{z_0} + 1\right) ,
$$

$$
\frac{\partial y}{\partial y_2} = \frac{1}{3}\left(0 + 1\right) = \frac{1}{3} , \text{ and}
$$

$$
\frac{\partial y}{\partial y_3} = \frac{1}{3}\left(\frac{zz_0}{\frac{2}{3}z_0^2} + 1\right) = \frac{1}{3}\left(\frac{3}{2}\frac{z}{z_0} + 1\right) . \tag{34}
$$

From equation 15 one then has

$$
\begin{aligned}
\Delta y(z) &= \sigma\sqrt{\sum_i \left(\frac{\partial y}{\partial y_i}\right)^2} \\
&= \sigma\sqrt{\frac{1}{9}\left(\frac{9}{4}\left(\frac{z}{z_0}\right)^2 - 3\frac{z}{z_0} + 1\right) + \frac{1}{9} + \frac{1}{9}\left(\frac{9}{4}\left(\frac{z}{z_0}\right)^2 + 3\frac{z}{z_0} + 1\right)} \\
&= \frac{\sigma}{\sqrt{3}}\cdot\sqrt{\frac{3}{2}\left(\frac{z}{z_0}\right)^2 + 1} . \tag{35}
\end{aligned}
$$

43